https://doi.org/10.5194/egusphere-2026-5161
Preprint. Discussion started: 14 September 2026

Lithological controls on seasonal freeze–thaw dynamics in coastal Antarctic permafrost: Insights from three years of continuous geophysical monitoring

Michaela Kňažková[1], Mohammad Farzamian[2,3], Filip Hrbáček[1], Teddi Herring[4], Tomáš Uxa[5,1], Christian Hauck[6]

[1]Department of Geography, Masaryk University, Brno, Czech Republic
[2]Instituto Nacional de Investigação Agrária e Veterinária, Oeiras, Portugal
[3]Institute of Geography and Spatial Planning, Universidade de Lisboa, Lisbon, Portugal
[4]Department of Civil Engineering, University of Calgary, Calgary, Canada
[5]Institute of Geophysics, Czech Academy of Sciences, Prague, Czech Republic
[6]Department of Geosciences, University of Fribourg, Fribourg, Switzerland

Correspondence to: Michaela Kňažková (michaelaknazkova@mail.muni.cz)

Abstract. An automated electrical resistivity tomography (A-ERT) system was installed in the vicinity of the Czech Johann Gregor Mendel Station on James Ross Island, Antarctica, in March 2023. The 23 m long transect crosses a lithological boundary between fine-grained Cretaceous sedimentary rocks and coarser marine terrace deposits, with daily electrical resistivity measurements complemented by environmental observation data. The aim of this study was to characterize the freeze–thaw dynamics of the active layer and explore the relationship between thermal, hydrological, and geoelectrical parameters in a geologically complex coastal permafrost environment. Three years of continuous monitoring have demonstrated that the two lithological units are markedly distinct in their geoelectrical response, with the electrical resistivity values consistently higher within the marine terrace section. In both lithologies, close relationships between electrical resistivity and ground temperature, as well as with soil moisture, were identified. A slight freezing point depression was detected, at −0.1 °C within the marine terrace deposits and −0.3 °C within the Cretaceous sediments. Tracking the progression of the thaw front was possible within the Cretaceous sediments using the gradient method; however, this proved challenging within the marine terrace deposits due to a greater vertical heterogeneity. This research demonstrates the usefulness of A-ERT as a tool for active layer and permafrost monitoring in complex settings, where traditional point- or borehole-based methods may not adequately represent spatial variability.

1 Introduction

Permafrost is a key component of the cryosphere and plays a significant role in shaping cold-climate landscapes. In recent decades, these regions have experienced accelerating rates of warming, with permafrost temperatures and active layer thickness responding sensitively to climatic variability. Variations in freeze–thaw dynamics can substantially affect surface hydrology, slope stability, and ecosystem functioning, making their monitoring crucial for understanding climate impacts in cold environments (Biskaborn et al., 2019; Obu, 2021). Therefore, the Global Climate Observing System (GCOS) has designated permafrost temperature and active layer thickness (ALT) as Essential Climate Variables (ECVs).

In Antarctica, permafrost is confined to the ice-free areas, which comprise only about 0.2% of the continent's total extent, covering approximately 45,000 to 55,000 km² (Brooks et al., 2019; Hrbáček et al., 2023a). Continuous permafrost is widespread across the coastal and island regions of the Antarctic Peninsula and adjacent archipelagos, transitioning to discontinuous permafrost primarily on the low-elevated parts of the South Shetland Islands (e.g. Bockheim et al., 2013). These ice-free regions are among the fastest-warming on Earth following a warming rate of 0.3–0.5 °C/decade (Turner et al., 2020), and with their extent projected to increase substantially by 2100 (Lee et al., 2017), their importance as important indicators of environmental change is increasingly being recognized (Vieira et al., 2010; Guglielmin and Cannone, 2012). The dynamics of the active layer in these environments is influenced not only by air temperature but also by snow cover, soil moisture, and substrate properties (Hrbáček et al., 2023). Monitoring the thermal and hydrological behaviour of the active layer is therefore critical for detecting early signs of permafrost degradation and for improving predictive models of permafrost response to ongoing climate change (Streletskiy et al., 2026).

Traditional active layer and permafrost monitoring methods, such as borehole temperature logging, thaw depth probing, or soil moisture measurements provide valuable long-term data but are limited in terms of spatial resolution and often constrained by logistical challenges in remote polar environments (Guglielmin, 2006). These point measurements, while essential, may also not adequately capture the spatial heterogeneity of subsurface conditions, particularly in geologically complex terrains. As a result, there is a growing need for complementary methods that can provide spatially distributed information on permafrost and active layer dynamics (Romanovsky et al., 2010; Hrbáček et al., 2023a).

Geophysical techniques, such as electrical resistivity tomography (ERT), have emerged as powerful tools for permafrost research. ERT is a non-invasive method that measures electrical resistivity of the ground, which is strongly influenced by its temperature, water, and ice content (Hauck, 2002). In frozen, ice-bearing ground, resistivity values are typically high due to the high electrical resistivity of ice, whereas thawed, water-saturated ground exhibits much lower resistivity (Hauck and Hilbich, 2024). This capability to distinguish between frozen and thawed substrates makes ERT particularly well-suited for detecting freeze–thaw transitions, mapping active layer thickness, or identifying zones of permafrost degradation (Mollaret et al., 2019).

While ERT has been widely used in permafrost studies, its application has traditionally been limited to discrete surveys conducted during field campaigns (Hilbich et al., 2008). In remote and logistically challenging environments such as Antarctica, repeated visits for data collection are often impractical or outright impossible due to high travel costs, limited accessibility especially during the austral winter season, and harsh weather conditions. These constraints have motivated the development of automated geophysical systems capable of continuous, year-round monitoring.

Automated electrical resistivity tomography (A-ERT) represents a significant advancement in this context (Farzamian et al., 2020, 2023). A-ERT systems combine conventional ERT with automated data acquisition and remote operation capabilities, allowing for high-frequency monitoring of subsurface resistivity without the need for regular human intervention (Hilbich et

https://doi.org/10.5194/egusphere-2026-5161
Preprint. Discussion started: 14 September 2026

al., 2011). These systems are specifically designed to operate under extreme environmental conditions, including sub-zero temperatures, strong winds, and high snow accumulation, making them particularly suitable for deployment in geographically isolated areas such as high mountains or Antarctica.

The first Antarctic deployment of an A-ERT system was conducted on Deception Island in the South Shetlands and it successfully demonstrated the feasibility of automated resistivity monitoring in a harsh polar environment (Farzamian et al., 2020). This pioneering effort laid the groundwork for further applications of the A-ERT technology in other, climatically and geologically distinct regions of Antarctica.

The Czech Antarctic Station Johann Gregor Mendel (JGM), situated on the northern coast of James Ross Island in the northeastern Antarctic Peninsula, has served as a long-term research hub for studying permafrost and active layer processes since 2006. Over two decades, the site has supported a growing network of air and ground temperature, and soil moisture sensors, as well as a CALM-S (Circumpolar Active Layer Monitoring–South) grid for probing active layer thickness (Brown et al., 2000; Hrbáček et al., 2017). These monitoring activities have produced a valuable multi-year dataset that has contributed to several studies on the thermal regime of permafrost (Hrbáček et al., 2017, 2021, 2025; Streletskiy et al., 2026) and the influence of environmental variables such as snow cover (Hrbáček et al., 2023a).

Recent findings from the CALM-S JGM site have highlighted the importance of lithological variability in controlling active layer dynamics (Hrbáček et al., 2025). In particular, contrasting thaw depths and moisture retention characteristics have been observed across different geological units, underscoring the need for spatially resolved investigations into the role of subsurface materials.

Moreover, uncertainties remain in accurately defining active layer boundaries. While traditional thermal monitoring provides essential baseline data, there is often a discrepancy between the position of the zero-degree isotherm and the depth of actually thawed ground due to freezing point depression and the shape of the freezing/thawing curve, which tends to be more gradual in fine substrates; a difference that can be on the order of tens of centimetres, especially in maritime environments affected by seawater intrusion or sea spray (e.g. Burn, 1998). Although this problem is known and has frequently been a topic for modelling or laboratory experiments (e.g. Devoie et al., 2022), field data documenting freezing point depression are rare (Tomaškovičová and Ingeman-Nielsen, 2024; Wang et al., 2026). Because electrical resistivity is highly sensitive to the phase state of soil water, the A-ERT method is able to more effectively distinguish between physically frozen and unfrozen ground, providing vital insights that thermal data alone cannot capture.

The deployment of the A-ERT system in March 2023 represents the latest step in the research trajectory on CALM-S JGM. The specific site of the A-ERT installation was selected to provide the potential for continuous, high-resolution monitoring of freeze–thaw processes, active layer evolution, and subsurface moisture dynamics across a transect with known lithological, moisture, and thaw depth contrast. This study presents the results after three years of monitoring and aims to demonstrate the value of A-ERT as a robust method for addressing the above-mentioned research gap and enhancing our understanding of permafrost and active layer, particularly in remote and data-scarce regions like Antarctica. Specifically, it focuses on three main objectives:

https://doi.org/10.5194/egusphere-2026-5161
Preprint. Discussion started: 14 September 2026

1. characterize the seasonal freeze–thaw dynamics of the active layer and associated temporal variability in electrical resistivity, with a focus on distinguishing between phase change and temperature-defined freeze–thaw thresholds,
2. explore the relationship among resistivity, temperature, and soil moisture, improving the interpretation of geophysical observations in terms of subsurface freeze–thaw processes, and
3. evaluate how contrasting lithology influences the spatial variability of freeze–thaw dynamics and the geophysical response within a coastal permafrost environment.

2 Methods

2.1 Study site

James Ross Island (JRI), located off the northeastern coast of the Antarctic Peninsula in the Weddell Sea (approx. 63.8°S, 57.9°W), is the largest island in the region. Covering an area of approximately 2,500 km², about one-quarter of its surface is currently ice-free, with deglaciation continuing throughout the Holocene (e.g. Roman et al., 2025). The location for this study was situated in the northern part of the island, the Ulu Peninsula, one of the largest continuous ice-free areas in the northern Antarctic Peninsula region (Fig. 1a).

The island lies at the climatic boundary between polar oceanic and polar continental zones and is underlain by continuous permafrost. Mean annual air temperatures are around −7 °C (Kaplan Pastíriková et al., 2023), with summer temperatures exceeding 0 °C and the sum of positive degree-days from 400 to 600 °C.days over the course of the thawing season, which lasts on average 100 days (Hrbáček et al., 2025). Annual precipitation is relatively low, estimated between 300 and 700 mm of water equivalent (van Wessem et al., 2016), and is predominantly snowfall. Strong prevailing winds from the south to southwest redistribute snow across the landscape, resulting in highly variable snow accumulation and meltwater availability (Kavan et al., 2020). This uneven distribution of moisture influences the sparse vegetation, which is limited to mosses and lichens forming small oases downstream of snowdrifts, while most of the terrain remains bare ground (Stringer et al., 2025).

The geological composition of JRI includes Cretaceous sedimentary rocks and Neogene to Quaternary volcanic formations (Mlčoch et al., 2020), overlain by unconsolidated marine, glacigenic, and fluvial deposits. The study site is located on the northern coast of the island, over a geological boundary dividing the Whisky Bay Formation sedimentary rocks (sandstones, mudstones) from Holocene marine terrace deposits. According to a texture analysis using wet sieving of material > 0.063 mm and the analysis of electrical conductivity in a 1:5 solution of distilled water, the sediments covering the Cretaceous Whisky Bay Formation are more fine-grained, with a higher silt and clay content and an electrical conductivity >1000 µS/cm. In contrast, the active layer covering the marine terrace consists predominantly of sandy material with low electrical conductivity. (Tab. 1).

Table 1. Characteristics of active layer texture and electrical conductivity (EC) in the two lithological units

https://doi.org/10.5194/egusphere-2026-5161
Preprint. Discussion started: 14 September 2026

unit	depth (cm)	sand (%)	silt and clay (%)	EC (μS/cm)
Cretaceous Whisky Bay Formation	5	43.0	57.0	1110
	30	53.8	46.2	825
	50	39.6	60.4	1150
	75	41.0	59.0	NA
Holocene marine terrace	5	75.9	24.1	45
	30	89.5	10.5	44
	50	94.0	6.0	50
	75	87.6	12.4	270

2.2 ERT surveys

Between 6 and 10 February 2023, two ERT profiles were conducted to characterize the general resistivity structure of the subsurface in the vicinity of the JGM Station (Fig. 1b). These surveys served for identifying suitable locations for long-term monitoring and as a baseline for interpreting the A-ERT data. The measurements were carried out using a 4POINTLIGHT_10W (Lippmann) resistivity meter, with 48 electrodes in the Wenner array. The longer profile spanned 324.5 m in length with an electrode spacing of 5.5 m, while the shorter profile was 59 m long with 1 m spacing. Data were processed using default settings in Res2DInv software with topographic correction derived from a local UAV-based digital elevation model.

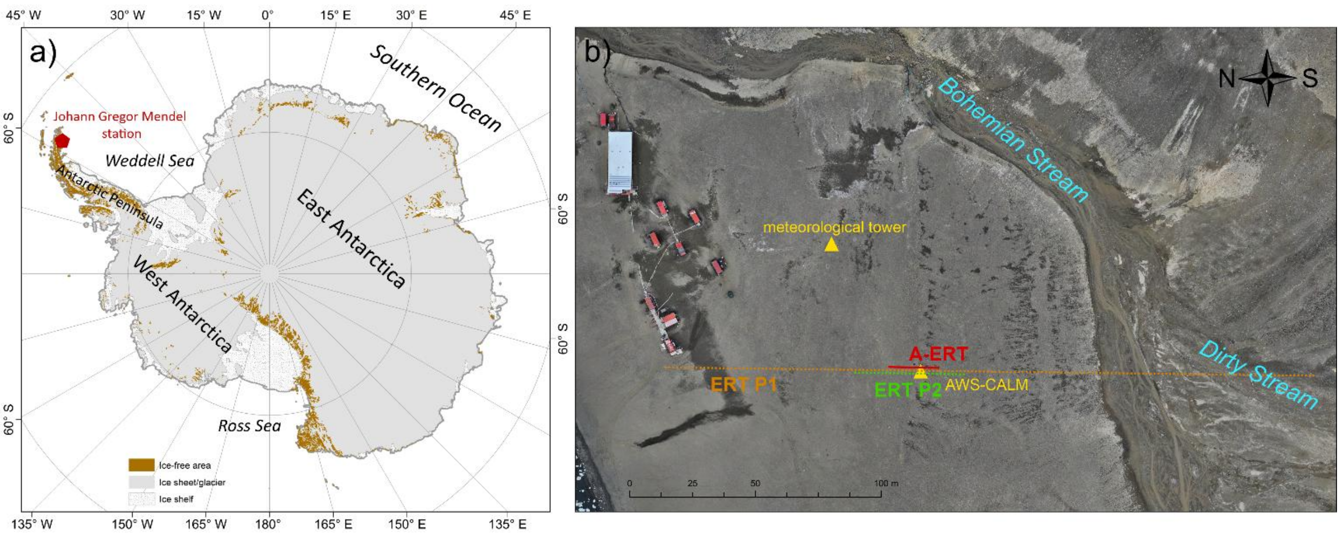

Figure 1: a) Location of the study site within Antarctica, b) aerial view of the surroundings of Johann Gregor Mendel station with the position of the A-ERT transect and ERT profiles.

https://doi.org/10.5194/egusphere-2026-5161
Preprint. Discussion started: 14 September 2026

2.3 A-ERT setup and data processing

2.3.1 A-ERT setup

The A-ERT system installed on JRI in late February 2023 is based on a 4POINTLIGHT_10W (Lippmann) resistivity meter, powered by a solar-charged battery system and equipped with an automated data logger (Farzamian et al., 2024a), and consists of 47 electrodes spaced at 0.5 m intervals along a 23 m transect. The surveys use the Wenner electrode configuration for optimized energy consumption and higher signal-to-noise ratio, yielding 347 individual data points for each monitoring dataset at 15 data levels, and a maximum investigation depth of approximately 4.5 m below the ground surface. The transect crosses the lithological boundary between the Holocene marine terrace deposits in the northern section and the weathered sedimentary rocks of the Cretaceous Whisky Bay Formation in the southern section, its elevation ranging from 10 to 12 m a.s.l. The marine terrace deposits overlay the Cretaceous sedimentary rocks and their thickness decreases with increasing distance from the shore, in the north–south direction. The surrounding terrain is predominantly flat, with minor depressions and scattered boulders that influence snow accumulation and meltwater redistribution, particularly during the early thawing season (Fig. 2). A-ERT measurements were started on 9 March and are recorded daily, with data retrieved during seasonal maintenance visits. For this study, data from 9 March 2023 to 2 March 2026 were analyzed, covering three full years and including two complete and two partial thawing seasons. Brief data gaps occurred due to interruptions during the seasonal maintenance visits for data download and system upgrades between 21 February and 2 March 2024, as well as between 23 January and 1 February 2025.

https://doi.org/10.5194/egusphere-2026-5161
Preprint. Discussion started: 14 September 2026

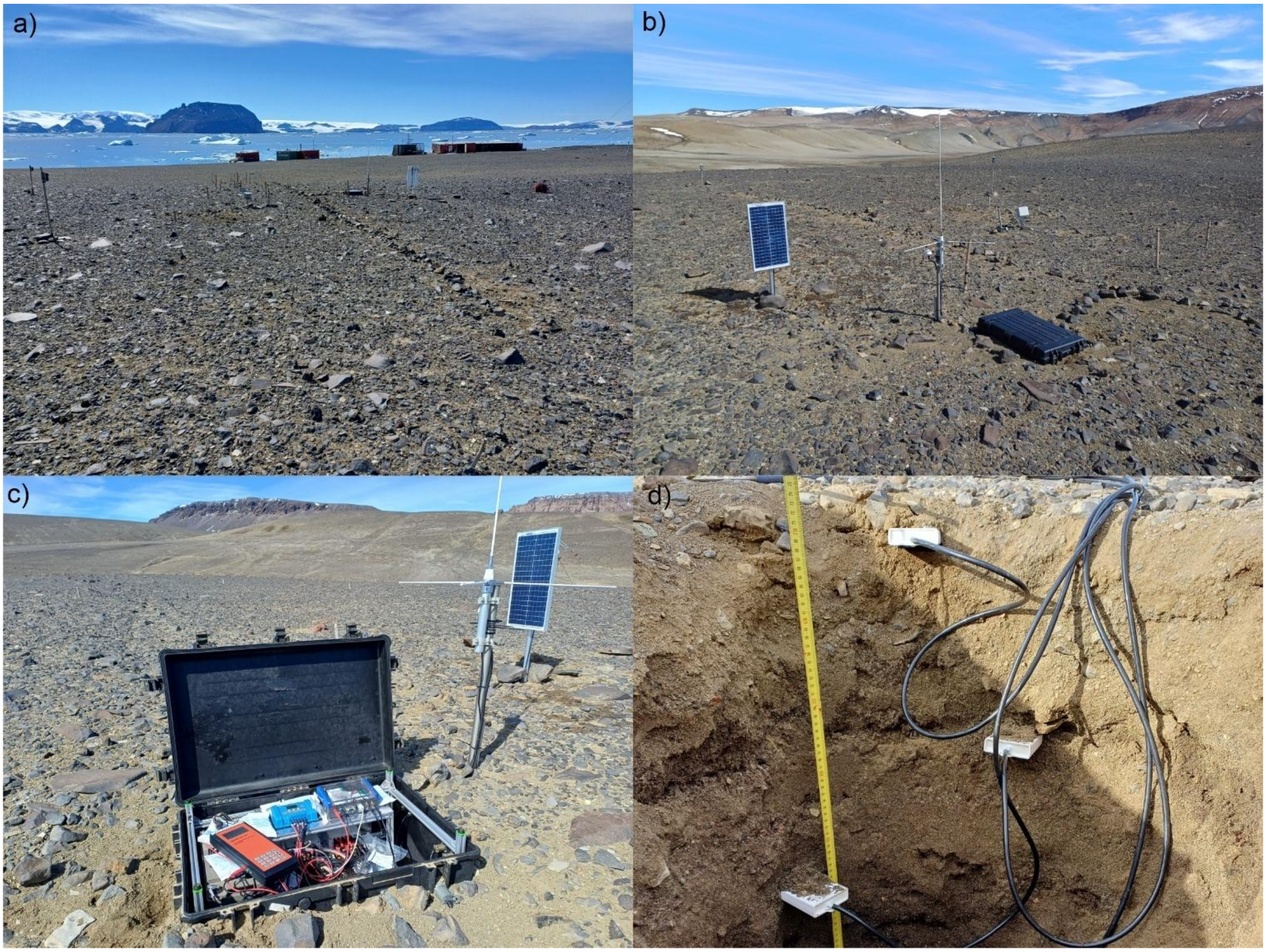

Figure 2: Photos of the A-ERT setup and the surrounding area – a) looking north towards the A-ERT transect and Johann Gregor Mendel station, b) the southern section of the transect, view towards the southwest, c) close-up of the A-ERT setup with the control unit, antenna and solar panel, d) installing TDR probes near the northern edge of the transect within the sandy marine terrace soil.

2.3.2 Data filtering and inversion

Following the framework adapted from Herring et al. (2023) and discussed in detail in Farzamian et al. (2024b), we applied a sequence of automated filtering steps based on empirically defined quality thresholds. These thresholds were fine-tuned through iterative testing on random data subsets to ensure consistent performance across all datasets. In the first step, measurements with negative apparent resistivities, stacking errors exceeding 2%, or extreme apparent resistivity values exceeding 9 standard deviations from the dataset distribution were removed. In step 2, a moving-median filter was applied to the logarithmic apparent resistivities along each pseudosection depth level using a five-point window. Points deviating by more than 7% from the local median were discarded. In step 3, electrodes producing unreliable measurements were flagged: if more than 30% of the data points related to a specific electrode were removed in earlier steps, all remaining data from this

https://doi.org/10.5194/egusphere-2026-5161
Preprint. Discussion started: 14 September 2026

electrode were excluded. Finally, in step 4, daily datasets with over 30% of points removed were rejected from inversion, as they were considered too degraded for reliable time-lapse interpretation.

Following data filtering, all measurements were inverted using pyGIMLi (Rücker et al., 2017) based on the procedures detailed in Farzamian et al. (2024). An L1 (blocky) model constraint was applied to enhance the resolution of sharp resistivity contrasts typical between thawed and frozen layers, the regularization parameter was optimized through the L-curve approach implemented in pyGIMLi (Günther et al., 2006), and data errors were modeled using a linear noise model with 4% relative noise and a 0.001 noise floor (Tso et al., 2017). Inversions were initialized with a homogeneous model using the average apparent resistivity of the first daily dataset and subsequently run in a cascaded mode, using each previous result as the starting model. The model coverage, derived from the normalized Jacobian, was used as an opacity filter to assess reliability.

In order to average the measured apparent resistivity values for individual depth levels, and plot their vertical and horizontal variability over time, electrode spacings were transformed into median investigation depths following Eq. (1), where a stands for electrode spacing (Loke, 2002).

$$z \approx 0.519 \times a \tag{1}$$

Relevant investigation depths were selected to represent surface (0.25 m), active layer/permafrost boundary (0.75 m), shallow permafrost (1.25 m), and deeper permafrost (3 m). Note that these calculated investigation depths do not correspond to actual depths, which can only be shown using inverted specific resistivities.

2.4 Environmental monitoring

To support the interpretation of resistivity data, air and ground temperature, and soil moisture data from long-term monitoring systems located within close range of the A-ERT transect were used. All sensors are installed within an approximately 2 m buffer from the transect to avoid interference with the A-ERT measurements, but at the same time ensuring comparability of the data. An overview of the environmental measurement setup is shown in Fig. 3.

The main ground temperature profile AWS-CALM is located slightly to the west from the centre of the transect within the Cretaceous sediments, where Pt100/8 thermistors were placed at depths of 5, 10, 20, 30, 50, 75, 100, 150, and 200 cm. These sensors were connected to an EdgeBox V12 data logger, and record data in 30-minute intervals. A secondary ground temperature profile (MT-75) was established near the northern edge of the transect, in order to measure ground temperatures within the marine terrace deposits in 30-minute intervals at 30, 50, and 75 cm. Instrumentation consists of Pt1000 thermistors connected to a MicroLog T3 data logger. Complementary air temperature data were obtained from a nearby meteorological tower (Fig. 1b), where it is measured at 2 m above ground using an EMS33 sensor housed in a radiation shield. All thermistors have ±0.15 °C accuracy. The sensors and data loggers for air and ground temperature monitoring were manufactured by EMS Brno.

Additionally, six Pt100/8 thermistors were placed at 5 cm depths in the northern (marine terrace) section to form a short transect parallel to the A-ERT line in an area frequently affected by snow accumulation. These sensors were utilized to detect the presence of snow, since even a relatively shallow snow cover effectively reduces the daily amplitude of ground temperature. All days with an amplitude lower than 1.5 °C were flagged as snow days. Visual confirmation was obtained using a network of trail cameras (Bunaty HD one; resolution 12 MPx) pointed at the northern and central part of the transect, as well as snow stakes deployed nearby, which also provided a rough estimate of snow depth.

Volumetric water content was measured using CS655 TDR probes (Campbell Scientific) with ±3% accuracy, connected to MicroLog T3 data loggers (EMS Brno). Two profiles (WB-TDR and MT-TDR, Fig. 3) were installed (one in each lithology), recording ground temperature and volumetric water content at depths of 5, 30, 50, and 75 cm at hourly intervals. The profile within the Cretaceous sediments spans the entire study period, while the profile in the marine terrace was operational from March 2024 onward, covering approximately two years. Besides volumetric water content, the probes also measure ground temperature with an accuracy of ±0.5 °C.

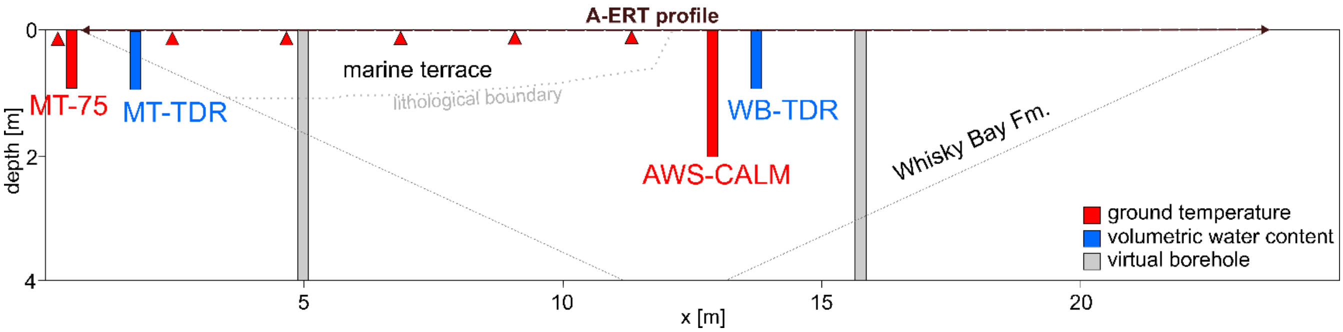

Figure 3: Lateral view of the transect (in the north–south direction from left to right) with schematic representation of the measurement setup (red triangles represent 5 cm ground temperature measurements) and the approximate position of the boundary between the two lithological units based on ERT surveys detailed in Sect. 3.1.

The environmental monitoring datasets were used to calculate active layer thickness (by interpolating the 0 °C isotherm between the bottommost positive and uppermost negative temperature depths; Hrbáček et al., 2025) and to correlate with A-ERT resistivity values by aligning the measurement times. To provide full context for the A-ERT measurements, which began near the end of the 2023 thawing season, environmental data collected from 1 October 2022 to 2 March 2026 were included in the analysis where available.

The study period was divided into sub-periods consisting of the individual thawing (December to February) and freezing (March to November) seasons. Seasonal and interannual (period of March to February to capture the full austral summer within one year) variability in ground thermal and moisture regimes was assessed using daily and seasonal averages.

Post-inversion analyses of A-ERT data include plotting resistivity variations along two virtual boreholes (one in the northern and one in the southern section of the transect, each in a distinct lithological setting) near x = 5 m and x = 16 m to track the temporal resistivity changes and compare them with ground temperature and volumetric water content data (cf. Fig. 3). In the case of x = 16 m, the resistivity data were related to the temperature in the main borehole AWS-CALM and to the WB-TDR soil moisture sensor located within the Cretaceous sediments, while the data from virtual borehole x = 5 m were complemented

https://doi.org/10.5194/egusphere-2026-5161
Preprint. Discussion started: 14 September 2026

with ground temperature data from the secondary borehole MT-75 and soil moisture data from the MT-TDR sensor, both installed within the marine terrace part of the transect (Fig. 3).

Additionally, the gradient method was applied in order to test whether the resistivity data can be efficiently utilized in predicting active layer thickness at our study site. This method has been developed to identify the interfaces between frozen and unfrozen material based on their large resistivity contrast (Herring and Lewkowicz, 2022). The results were compared with ALT values obtained by interpolating the depth of the 0 °C isotherm.

3 Results

3.1 ERT surveys

The longer profile shows a complex subsurface structure with zones of relatively high resistivity (~150–300 Ωm) interpreted as solid Cretaceous bedrock, interspersed with zones of lower resistivity (~100–150 Ωm) interpreted as the same material in different stages of consolidation. Extremely low resistivity values (below ~50 Ωm) were measured in the joint braidplain of the Bohemian and Dirty streams to the south, due to the waterlogged nature of the fluvial sediments (Fig. 4a). In this configuration, neither the active layer nor the boundary between the sedimentary rocks of the Whisky Bay Formation and the Holocene marine terrace, which is likely less than 2.5 m thick, was detected. In the northern part of the profile, areas of lower resistivity at the surface correspond to different stages of weathering of the Cretaceous rocks.

The shorter, high-resolution profile with 1 m electrode spacing provides a more detailed image of the lithological boundary. At its northern end, the marine terrace deposits are estimated to be about 1 m thick, characterized by high resistivity values (> 100 Ωm), and underlain by weathered Cretaceous bedrock of lower resistivity (~50 Ωm). The southern section is marked by a sharp resistivity contrast between the loose regolith at the surface and the underlying bedrock (Fig. 4b).

https://doi.org/10.5194/egusphere-2026-5161
Preprint. Discussion started: 14 September 2026

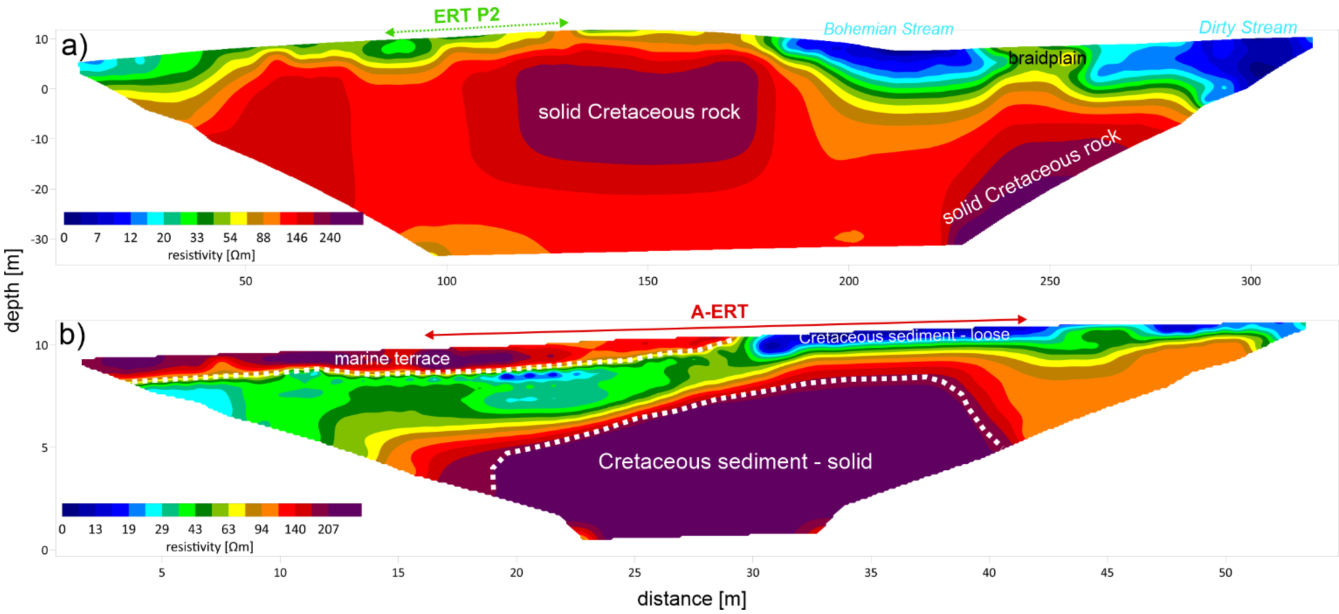

Figure 4: Overview of the ERT surveys in the vicinity of JGM station – a) ERT P1 profile (longer), b) ERT P2 profile (shorter), both oriented from north to south (left to right).

3.2 Environmental observations

3.2.1 Air and ground temperature

The variability of the annual and seasonal air and ground thermal regimes in the period from 1 October 2022 to 28 February 2026 is summarized in Tab. 2 and Fig. 5a, b.

Overall, the differences between the three monitoring years were quite pronounced. Air and ground temperatures fluctuated substantially during the study period, with 2024/2025 being the coldest year. Between 2023/2024 and 2024/2025, mean annual air temperature decreased from −4.8 °C to −7.0 °C, and then increased again to −4.0 °C in 2025/2026. Ground temperatures at all depths showed a similar pattern, with mean annual ground temperature at 5 cm depth (GT5) dropping from −3.8 °C in 2023/2024 to −5.5 °C in 2024/2025, before rising to −3.3 °C in 2025/2026.

The freezing seasons (FS) also exhibited notable variations. Mean air temperature dropped from −6.9 °C in 2023 to −9.4 °C in 2024. Ground temperatures at all depths followed the same pattern, with mean GT5 decreasing from −6.8 °C in 2023 to −8.7 °C in 2024, and mean GT200 from −4.4 °C in 2023 to −5.9 °C in 2024. However, the freezing season of 2025 was the warmest out of the three (Tab. 2, Fig. 5b).

The thawing season (TS) mean air temperature decreased from 1.9 °C in 2022/2023 to 0.3 °C in 2024/2025, and mean GT5 followed a similar pattern, decreasing from 5.8 °C to 4.3 °C. While the very last thawing season was slightly warmer in terms of air temperature, this was not reflected in the ground temperatures down to 75 cm, where the cooling of the previous thawing seasons continued. On the other hand, the deeper layers of ground warmed interannually, possibly in response to the mild freezing season of 2025 (Tab. 2).

https://doi.org/10.5194/egusphere-2026-5161
Preprint. Discussion started: 14 September 2026

Importantly, these thermal regime shifts have had a direct impact on active layer thickness (ALT), which decreased gradually from 98 cm in 2022/2023 to 84 cm in 2025/2026, based on the zero-degree isotherm position within the main borehole AWS-CALM. This thinning of 14 cm reflects the cumulative effect of cooler thawing seasons and more intense freezing following the 2024 season, resulting in a shallower seasonal thaw depth.

Variations in mean daily air temperature are extremely high on JRI, especially during the winter, frequently exhibiting rapid drops. In the absence of snow cover, these warm spells penetrate more easily into the ground, resulting in near-surface temperatures approaching 0 °C. In extreme cases, surface thawing may occur, such as in late August and September of 2025 (Fig. 5a).

Table 2. Summary of air and ground thermal regime during the study period at AWS-CALM

	AT	GT_5	GT_{75}	GT_{200}	ALT
TS 2022/2023	1.9	5.8	0.3	−2.5	98
TS 2023/2024	1.5	5.2	−0.4	−2.9	95
TS 2024/2025	0.3	4.3	−0.6	−3.4	87
TS 2025/2026	0.8	4.1	−0.9	−3.0	84
FS 2023	−6.9	−6.8	−5.2	−4.4	-
FS 2024	−9.4	−8.7	−7.1	−5.9	-
FS 2025	−5.6	−5.7	−4.6	−4.3	-
2023/2024	−4.8	−3.8	−4.0	−4.0	-
2024/2025	−7.0	−5.5	−5.5	−5.3	-
2025/2026	−4.3	−3.3	−3.7	−4.0	-

https://doi.org/10.5194/egusphere-2026-5161
Preprint. Discussion started: 14 September 2026

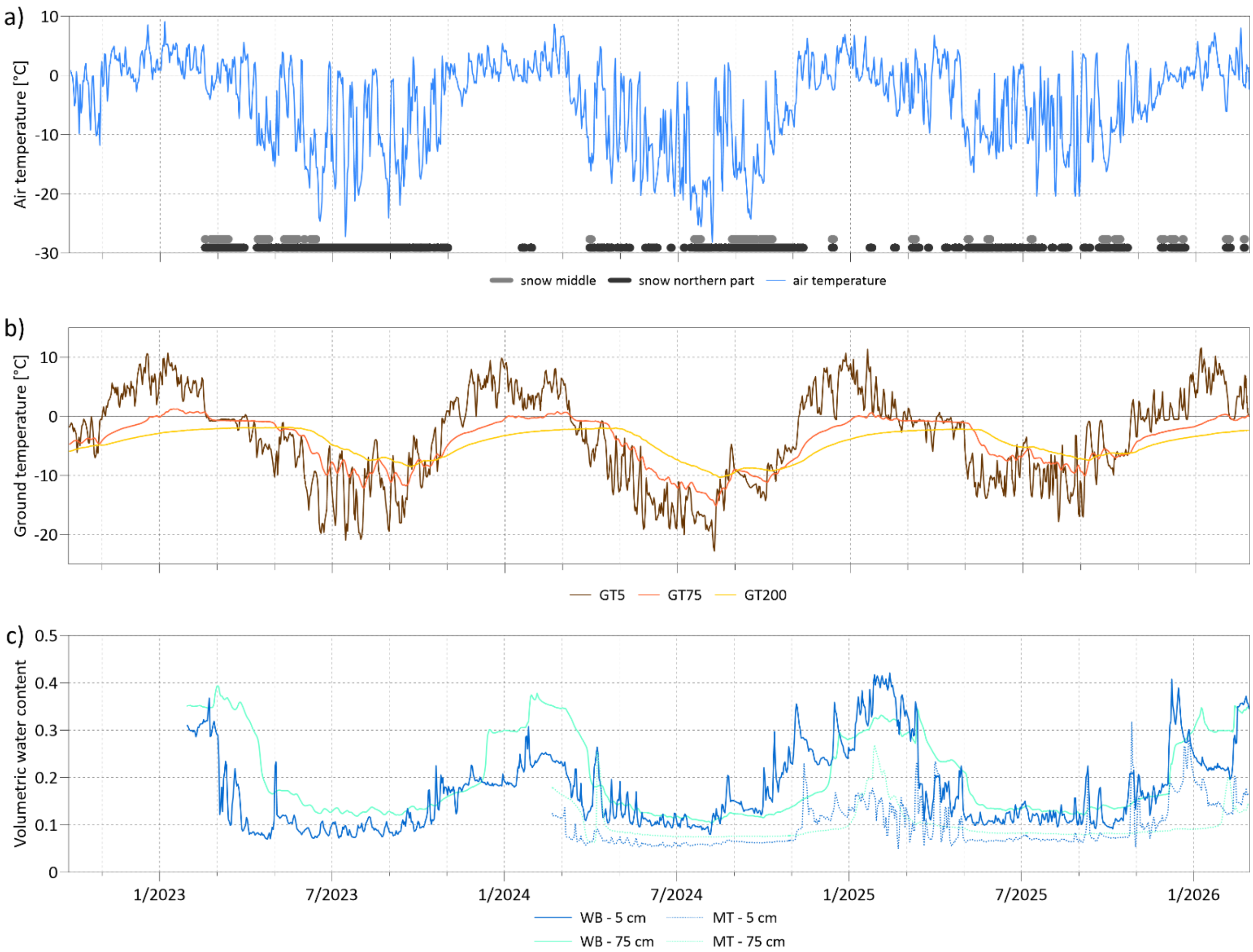

Figure 5: a) Interannual variability of daily averages of air temperature over the study period, grey dots indicate the presence of snow in the northern and middle sections of the A-ERT profile; b) daily variability of ground temperature within the main borehole AWS-CALM located in the Cretaceous sediments; c) daily variability of volumetric water content within the two profiles WB-TDR (Cretaceous sediments) and MT-TDR (marine terrace).

3.2.2 Snow cover

In general, snow accumulations on JRI do not exceed 30 cm in flat areas, and they are commonly interspersed with bare patches (Fig. 6b). The snowpacks lasting several months are frequently only 5–10 cm deep. Due to favourable topography and the predominant direction of the wind from south to southwest, driving the snow to accumulate downwind from the lithological boundary and onto the gently inclined marine terrace, the northern part of the A-ERT transect is more commonly covered by snow during late winter and early summer (Fig. 6a). Meanwhile, there are pronounced differences in the duration of seasonal snow cover between the individual winter seasons (Fig. 5a). The total number of days with snow cover was by far the highest during 2023, when snow persisted for 233 days in the northern part and for 71 days in the middle part between February and

https://doi.org/10.5194/egusphere-2026-5161
Preprint. Discussion started: 14 September 2026

October. Notably, snowfall occurred during the ground freezing phase in early March and affected the length of the zero-curtain period. This initial snowpack almost completely melted during a brief warm spell in early April, but from mid-April onwards, snow cover persisted for most of the winter period in the northern part, while the central part of the profile was largely snow-free.

In the winter of 2024, there were 53 snow days in the central part of the profile and 156 in the northern part, which was two and a half months less than the previous year. Larger snowfall events only occurred during late July and August. As a result, there were prolonged periods especially at the beginning of winter when the ground was entirely snow-free. However, the snow cover lasted the longest into the thawing season, and only melted completely in mid-November. The winter of 2025 was comparable in terms of snow days (38 and 150 days in the central and northern parts, respectively), but with more irregular distribution across the season, so that the ground was never completely snow-covered for more than a month. Most of the snow was lost due to sublimation and wind redistribution instead of melting in situ at the beginning of the thawing season.

The occurrence of snow during the thawing season on JRI is quite rare and short-lived. However, there was a notably high number of snow days during the thawing season 2025/2026 (18 and 28 days for the central and northern parts, respectively) compared to the previous years (3 and 10 days in 2023/2024; 6 and 14 days in 2024/2025 for the central and northern parts, respectively). This unusually long persistence of snow might have contributed to the overall thinner active layer, particularly since several snowfall events occurred in early to mid-February, at a time when maximum seasonal thaw depths are normally observed (Fig. 5a).

https://doi.org/10.5194/egusphere-2026-5161
Preprint. Discussion started: 14 September 2026

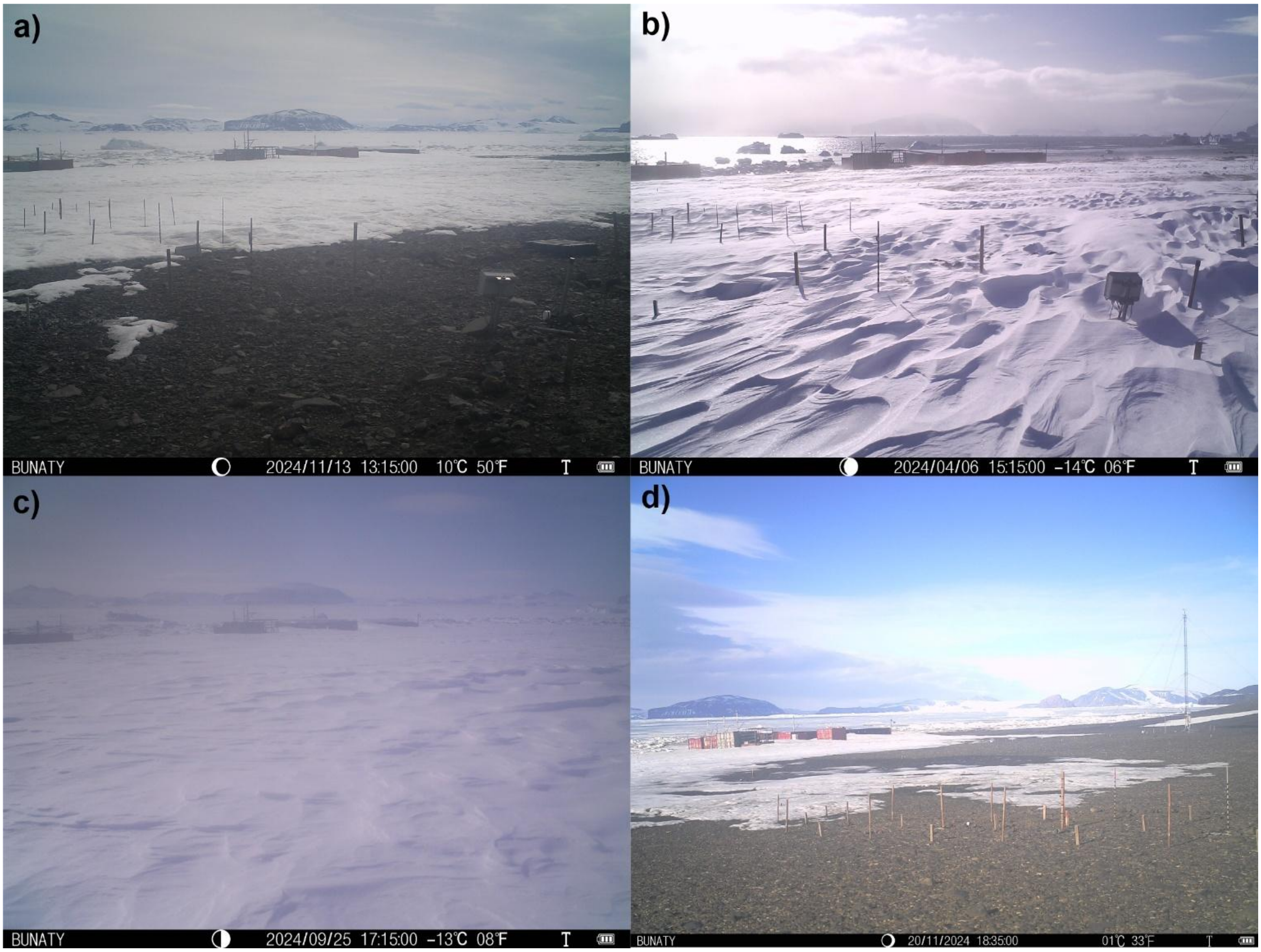

Figure 6: Trail camera photos illustrating the typical snow cover patterns on JRI – a) snow covering only the northern section of the A-ERT transect, most common; b) irregular, wind-blown snow cover with deep snowdrifts and bare ground peeking through within the troughs; c) snowfall during the late days of winter 2024 – a rare occasion when snow cover thickness exceeds stake height; d) snowmelt draining downhill from the A-ERT transect (darker zone of saturation visible).

3.2.3 Volumetric water content

Both profiles measuring volumetric water content show seasonal variability across the monitored depths, with higher overall variability within the surface layer and during the thawing season, driven predominantly by meltwater infiltration and occasional rain events. During the freezing season, the levels of unfrozen water content exhibit reduced variability dependent on ground temperature alone (Fig. 5c).

The profile located within the Cretaceous sediments consistently shows higher soil moisture levels throughout the year, with pronounced differences between the freezing and thawing seasons. Although this part of the transect receives less meltwater from snow in general, higher water content values are observed due to the overall greater water-retaining capacity of the fine-grained substrate (Tab. 1). Peak values in the unfrozen soil might exceed 0.4 cm^3/cm^3, especially in the surface layer. During the freezing season, unfrozen water content ranged from approximately 0.07 to 0.13 cm^3/cm^3, with lower values in the shallower layers and higher values in the deeper parts of the profile based on frost penetration. Distinct peaks occur particularly at the onset of the thawing season, when the soil might become saturated more easily with snowmelt due to the still frozen layers underneath. Differences between the individual years are also quite pronounced. During the thawing season of 2023/2024, a notable deficit of moisture was observed within the surface layer compared to the subsurface, while the situation was quite different during the following year, when the distribution of moisture within the profile was much more uniform (Fig. 5c). This might be attributed to a more prolonged occurrence of snow in the second part of winter in 2024, while the central part of the profile was entirely snow-free in 2023 from July onwards.

In contrast, the profile situated in marine terrace sediments displayed generally lower moisture levels despite a more prolonged presence of snow in general, ranging from 0.04 to slightly over 0.3 cm^3/cm^3. The variability in the surface layer was also somewhat reduced compared to WB-TDR and while distinct peaks appear at the beginning of the thawing season, the meltwater is more rapidly drained downwards within the soil and also downhill away from the transect due to the lower water-retaining capacity of the coarser substrate. During the freezing season, unfrozen water content is also lower than within the Cretaceous sediments and remains relatively stable, ranging only very slightly from 0.04 to 0.07 cm^3/cm^3 across the profile (Fig. 5c).

3.3 Apparent electrical resistivity variability

3.3.1 Variability along the profile

Apparent electrical resistivity data reveal distinct responses of the two main lithological units separated by a transitional zone that was excluded from the average in order to not skew the values of either segment (Fig. 3). For the purposes of analysis, the transect was therefore divided into three parts based on the variability in apparent resistivity values (Fig. 7).

1. Holocene marine terrace ($x = 0.75–9.25$ m) – northern segment exhibits consistently higher resistivity values, frequently exceeding 2500 Ωm during the freezing season, and substantial variability, indicating subsurface conditions associated with a resistive lithology such as coarse-grained sediments,
2. Transitional zone ($x \approx 9.75–13.75$ m) – gradual decline compared to the marine terrace in both median resistivity and variability, representing a geological gradient or a mixing zone, where the properties of the two lithological units overlap,
3. Cretaceous sediments ($x = 14.25–22.25$ m) – southern segment, where the resistivity values remain consistently lower, rarely exceeding 1500 Ωm, and variability is reduced, suggesting a more conductive and uniform lithology, indicative of finer-grained materials and higher unfrozen water content in winter.

https://doi.org/10.5194/egusphere-2026-5161
Preprint. Discussion started: 14 September 2026

3.3.2 Annual and seasonal variability

Measurements of apparent electrical resistivity exhibit pronounced variability between the thawing and freezing seasons and inversely follow the fluctuations of ground temperature. Generally, the resistivity values decline sharply during the austral summer as thawing begins, followed by a substantial rise at the onset of the freezing season. At greater investigation depths, this physical response features a distinct time lag alongside a dampening of apparent resistivity amplitude (Fig. 7). While the shallowest layers (0.25 m and 0.75 m) react almost instantaneously to temperature fluctuations with steep resistivity changes, the 3 m depth experiences a lag of several months. Consequently, deep resistivity often reaches its peak (approximately 400 to 500 Ωm) late in the year just as the near-surface layers are already undergoing rapid thaw.

Although all three monitoring years exhibit this overarching trend, the exact timing and scale of individual peaks vary greatly depending on the precise onset dates of the seasonal transitions, the severity of the thawing and freezing seasons, and actual moisture levels within the ground.

The timing of the onset of seasonal freezing differs markedly between the individual years, heavily impacting the initial resistivity gradients. In 2023, a relatively long zero-curtain period (lasting from late February to early April, characterized by continuous snow cover) was followed by the full onset of the freezing season between mid-April and mid-May. This transition is striking in both lithological segments, with the 0.25 m depth surging rapidly from summer baselines (around 100 Ωm in the marine terrace and 50 Ωm in the Cretaceous sediments) to over 500 Ωm within just a few weeks, before a brief late-May warming temporarily reversed the trend. In contrast, the zero-curtain period in 2024 was cut drastically shorter in the absence of snow cover, shifting the freezing onset earlier by approximately three weeks. This resulted in an even steeper initial change, with shallow resistivity climbing to 1000 Ωm at an accelerated rate compared to the previous year. The zero-curtain period in 2025 was the longest at almost eight weeks. Consequently, the onset of freezing and the subsequent resistivity increase shifted to as late as early May. The ascent in the resistivity values was notably more gradual; particularly in the Cretaceous sediments (Fig. 7b), the values struggled to differentiate by depth during the early freeze, climbing at a much slower rate than in the marine terrace.

Maximum values during the peak winter period (July to September) within the surface layer vary greatly according to the profile segment. Driven by ground temperatures frequently fluctuating between −5 °C and −20 °C at 5 cm depth, the resistivity values peaked in mid-August 2024 at approximately 2000 Ωm in the marine terrace and 1200 Ωm in the Cretaceous sediments. Toward the end of the 2024 winter, widespread snow cover insulated the profile, reducing the amplitude of temperature fluctuations and stabilizing apparent resistivity values. Conversely, during the exceptionally warm 2025 freezing season, surface layer values were approximately 500 Ωm lower overall than in the previous two seasons. For almost the entire duration of this winter, values within the Cretaceous sediments were exceptionally low and remarkably homogeneous across all depths, clustering tightly between 200 and 300 Ωm (Fig. 7b). This dramatic reduction, particularly in the shallower layers, might be attributed to higher unfrozen water content alongside the unusually warm winter temperatures; during September, the ground came very close to actual thawing conditions.

https://doi.org/10.5194/egusphere-2026-5161
Preprint. Discussion started: 14 September 2026

The onset of the thawing season usually occurs in late October to mid-November and is characterized by a sharp decline in the apparent resistivity values across the active layer. During this brief window, values at the 0.25 m and 0.75 m depths plummet from their winter highs of >1000 Ωm back down to their summer baselines (below 100 Ωm in the marine terrace and below 20 Ωm in the Cretaceous sediments). This rapid near-surface thaw creates a distinct and recurring depth inversion in the dataset: as the shallow layers become highly conductive with more liquid moisture content, their resistivity drops below that of the deeper 1.25 m and 3 m layers, which remain frozen and more resistive (>300 Ωm) well into the summer before gradually warming. Specific dates for the onset and duration of freezing and thawing seasons are further illustrated in Fig. 8 and described in Sect. 3.4.1 in relation to inverted values of electrical resistivity.

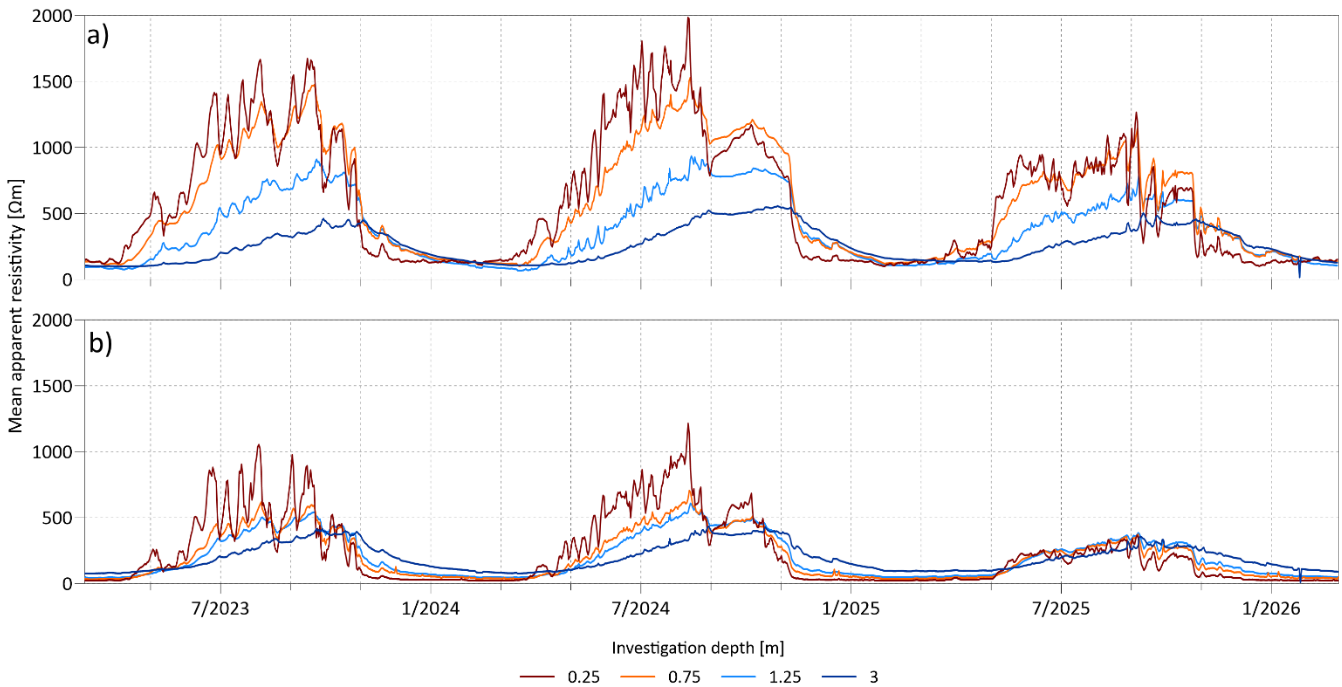

Figure 7: Variability of apparent electrical resistivity (spatial mean value over a profile segment) for a) marine terrace and b) Cretaceous sediments segments of the transect and different investigation depths over the three-year study period.

3.4 Inverted resistivity models

3.4.1 2D models

Inverted 2D models of the electrical resistivity distribution within the profile during different phases relevant to the ground thermal regime were selected. These include the onset of the freezing (Fig. 8a) and thawing (Fig. 8d) phases, the occurrence of maximum (Fig. 8e, f) and minimum temperatures (Fig. 8b), and conditions approaching isothermal states (Fig. 8c), when the temperature difference within the borehole AWS-CALM is minimal.

In most cases, the 2D tomograms distinguish well between both lithologies in the topmost 0.75–1 m, corresponding approximately to the long-term depth of the active layer. In general, the left (northern) part of the profile formed in the topmost

https://doi.org/10.5194/egusphere-2026-5161
Preprint. Discussion started: 14 September 2026

1 to 1.5 m by marine terrace sediments is more resistive than the Cretaceous sediments on the right (southern part). Particularly during the freezing phase (Fig. 8b, c), the higher resistivities (up to 2500 Ωm) in the marine terrace soil create a clear contrast to the less resistive Cretaceous sediments (ca. 1000 Ωm). Similarly, the values during the thawing phase (Fig. 8d–f) are around 100–150 Ωm in the marine terrace and drop to 10–30 Ωm within the Cretaceous sediments. In some cases (Figs. 8b, c, f), it is possible to detect a very thin surficial layer (0–0.2 m) in the left part of the profile, which exhibits lower resistivity than the underlying bulk of the marine terrace sediments.

The 2D tomograms clearly capture the pronounced interannual differences in winter severity and the resulting ground response. The freezing season of 2024 stands out as the most extreme, with surface temperatures plummeting to −22.8 °C and temperatures at 2 m depth reaching −9.5 °C. This pushed resistivity values to their absolute peaks (~3000 Ωm) deep in the profile, particularly within the marine terrace. In stark contrast, the minimum temperatures recorded in 2025 were significantly higher (−16.5 °C at the surface and −6.0 °C at 2 m depth). This warmer winter is visually striking in the tomogram, displaying markedly lower bulk resistivities across both lithologies, directly corroborating the overall 500 Ωm reduction observed in the apparent resistivity data. Furthermore, under near-isothermal conditions (Fig. 8c), the profile reached a perfect −9.0 °C equilibrium in September 2024, allowing for the effect of lithological differences to take precedence and maintaining a highly resistive frozen state, whereas the warmer −5.6 °C to −6.0 °C equilibrium in October 2025 yielded a visibly more conductive subsurface.

Just as winter extremes varied, the thawing phases showcased significant interannual variations in timing and intensity. The onset of the thawing season (Fig. 8d) was significantly delayed in 2024 by the presence of snow, with the surface still frozen at −1.3 °C in mid-November and high resistivities dominating particularly in the marine terrace. Conversely, by late October 2025, the surface had already warmed to 4.3 °C, triggering an immediate and rapid development of a highly conductive active layer. This early thaw culminated in an exceptionally warm summer peak in January 2026 (Fig. 8e), where surface temperatures reached 18.2 °C, which doubled the 9.1 °C maximum of the previous year. However, despite this extreme heat, the active layer was visibly thinner than in the previous year, albeit more conductive, dropping to 10 Ωm in the Cretaceous sediments.

Below the active layer, the deeper permafrost layer below 1.5 m depth is assumed to be formed solely of Cretaceous sediments. The resistivity of the permafrost at a depth of 2 m gradually increases from the northern (30–300 Ωm) to the southern part (50–500 Ωm) of the transect. The area in the middle part of the transect that shows contrasting resistivity, especially in the winter season (Fig. 8b, c), which suggests a regular shape with a nearly vertical boundary, is considered to be an artifact of the inversion modelling.

https://doi.org/10.5194/egusphere-2026-5161
Preprint. Discussion started: 14 September 2026

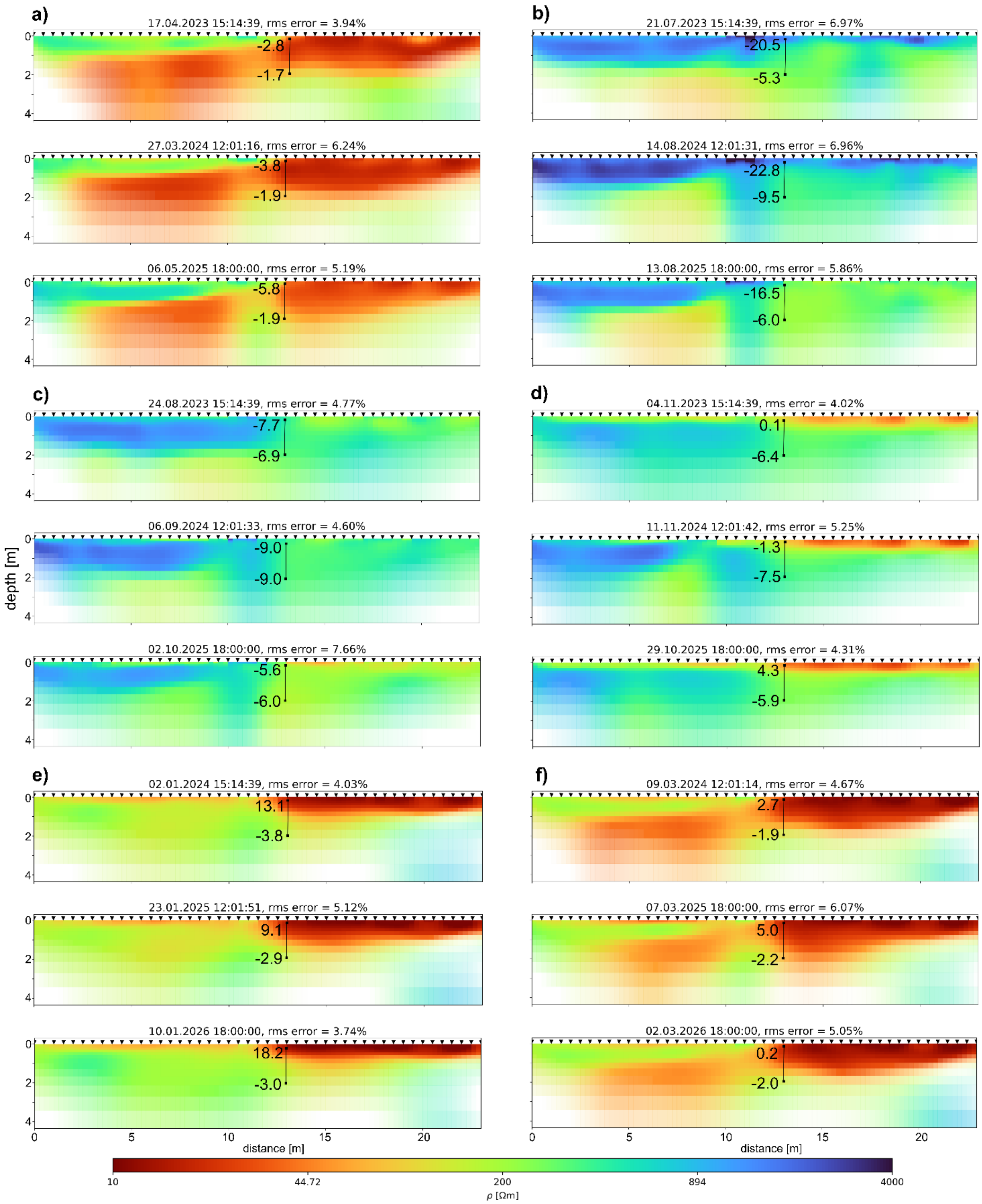

430

https://doi.org/10.5194/egusphere-2026-5161
Preprint. Discussion started: 14 September 2026

Figure 8: Inverted 2D models of electrical resistivity in the seasons 2023/2024, 2024/2025, and 2025/2026 during the a) onset of freezing towards the end of zero-curtain period, b) lowest winter temperatures, c) isothermal conditions, d) onset of thawing, e) highest surface temperatures (maximum of GT5), and f) highest subsurface temperatures (maximum of GT100). Overlain are the GT5 and GT200 temperatures from the AWS-CALM borehole.

3.4.2 Virtual boreholes and ALT

To continuously track these interannual and depth-dependent dynamics, 1D virtual boreholes were extracted from the inverted time-lapse ERT data at x = 5 m (representing the marine terrace) and x = 16 m (representing the Cretaceous sediments). Both virtual boreholes (Fig. 9a) corroborate the patterns observed in the apparent resistivity and 2D models, such as a significant year-to-year decrease in peak winter resistivity values between the 2023/2024 season and the exceptionally warm 2025/2026 season. Despite this interannual winter warming tendency, the main vertical resistivity patterns remained the same in the two lithologies.

At x = 5 m (marine terrace), the zone of highest resistivity is concentrated in a highly resistive frozen layer located between depths of 40 and 120 cm. The maximum values within this layer steadily decreased from approximately 3000 Ωm in 2023/2024 down to 1800 Ωm in 2025/2026. Below a depth of 150 cm, the resistivity values drop significantly. This vertical boundary reflects the transition from the coarse marine terrace deposits into the underlying and more conductive Cretaceous sediments (as previously detailed in Figs. 3 and 4).

At x = 16 m (Cretaceous sediments), the vertical profile is much more uniform, lacking the resistive overlying terrace, with resistivity gradually decreasing from the surface down to greater depths. The maximum values in the surficial layer experienced a severe interannual drop, plunging from approximately 1500 Ωm in 2023/2024 to just 500 Ωm in 2025/2026. At deeper levels (e.g. 200 cm), the ground dampens this year-to-year change, resulting in a minor maximum decrease from 500 to 400 Ωm.

To assess the depth of the active layer, Fig. 9a shows the reference ALT defined by the exact depth of the 0 °C isotherm compared against the maximum vertical resistivity gradient identified using the gradient method introduced by Herring and Lewkowicz (2022). This approach chooses the depth of maximum resistivity gradient as the most probable active layer depth, rather than defining a rigid threshold that can be very different in different lithologies. The reference 0 °C isotherm data show a highly consistent seasonal evolution in terms of the onset, peak, and end of the thawing season across both boreholes, with the absolute ALT difference between the two lithologies of approximately 10–15 cm. However, applying the resistivity gradient method to estimate ALT yielded strong discrepancies depending on the geological material.

At x = 5 m, the gradient method fails to capture the true thaw depth in the marine terrace, severely underestimating the ALT compared to the 0 °C isotherm. The algorithm tends to lock onto a shallow depth, estimating an ALT of only about 25 cm across all seasons, and even shows a decrease between the early and peak thawing periods. In the more vertically homogeneous Cretaceous sediments, the gradient method performs significantly better during the early thawing season, faithfully tracking the downward progression of the 0 °C isotherm. However, during the peak of the thawing season, the method severely overestimates the ALT by approximately 80 cm (Fig. 9a).

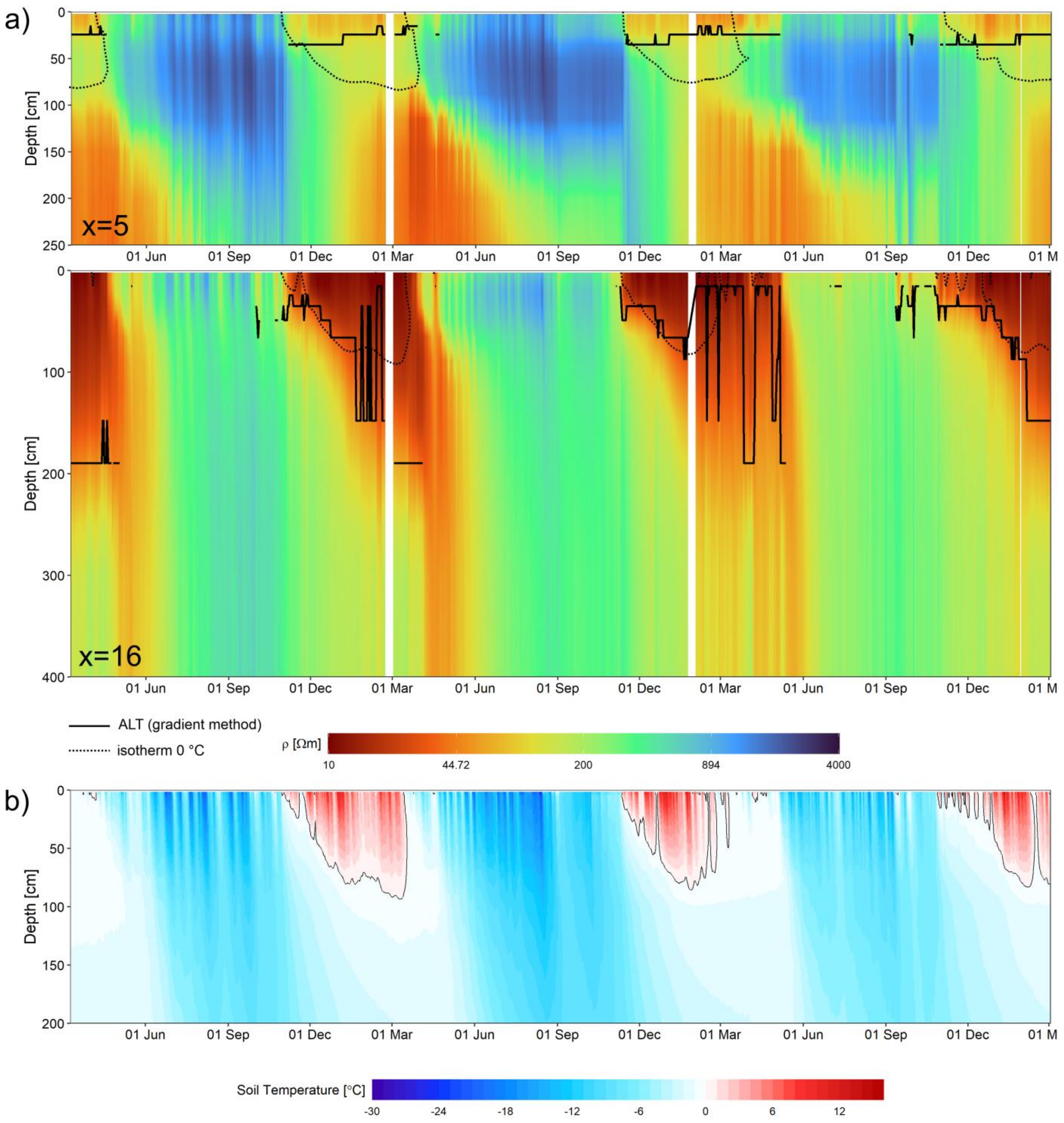

465 **Figure 9: a) Vertical distribution of electrical resistivity within the two virtual boreholes during the three years of monitoring, including evolution of ALT based on the gradient method and the position of the 0 °C isotherm; b) daily variability of ground temperature within the AWS-CALM borehole.**

3.5 Relationship between electrical resistivity, temperature, and water content

To explain the spatial contrasts in the 2D tomograms and the discrepancies in ALT estimations, the physical relationships between ground temperature, volumetric water content, and electrical resistivity were evaluated at a depth of 75 cm (Fig. 10). Because electrical resistivity in frozen ground is largely controlled by the unfrozen water content, the exact temperature at which bulk freezing occurs is critical. The freezing point at 75 cm is estimated at −0.3 °C in the Cretaceous sediments and −0.1 °C in the Holocene sediments. As temperatures continue to drop, the termination of the zero-curtain period (documented by a pronounced, steep inflection on both the temperature vs. moisture and temperature vs. resistivity curves) is estimated at −0.7 °C for the Cretaceous sediments and −0.2 °C for the marine terrace. This delayed phase transition in the Cretaceous material allows these finer-grained sediments to retain a substantial amount of highly conductive unfrozen water at sub-zero temperatures. Conversely, the coarser marine terrace sediments freeze and thaw almost instantaneously near 0 °C.

The continuous freeze–thaw curves (Fig. 10) demonstrate a hysteresis loop, where lower temperatures are required to force initial freezing (due to pore-scale supercooling effects) than to initiate thawing. As a result, the zero-curtain onset temperature during the spring thaw is much closer to 0 °C in both lithologies.

Crucially, while the previous sections highlighted the interannual variability in peak winter resistivity and overall ground temperatures between 2023/2024 and 2025/2026, the thermodynamic boundaries remain remarkably stable. Even though there are noticeable year-to-year differences in the initial water content prior to freezing and the absolute volume of unfrozen water during peak winter, no measurable effect on the initiation temperature of the thawing zero-curtain was detected. This confirms that while maximum resistivity values are highly sensitive to interannual temperature variations, the critical temperature thresholds for phase transitions are fixed strictly by lithology.

These distinct thermal properties yield fundamentally different baseline resistivity thresholds for phase changes. In the Cretaceous sediments, the resistivity values corresponding to the freezing point and zero-curtain onset form tightly clustered, predictable curves, ranging from roughly 20 Ωm (during the warmer 2025/2026 season) to 30 Ωm (2023/2024). Slightly higher resistivity marks the zero-curtain termination, ranging from 25 Ωm to 40 Ωm. In sharp contrast, establishing clear resistivity thresholds for the marine terrace sediments is highly complex due to intense data scattering within the critical temperature interval of 0 °C to −2.5 °C. An approximate estimate of the phase-change threshold for the marine terrace sits vastly higher, around 150–250 Ωm.

https://doi.org/10.5194/egusphere-2026-5161
Preprint. Discussion started: 14 September 2026

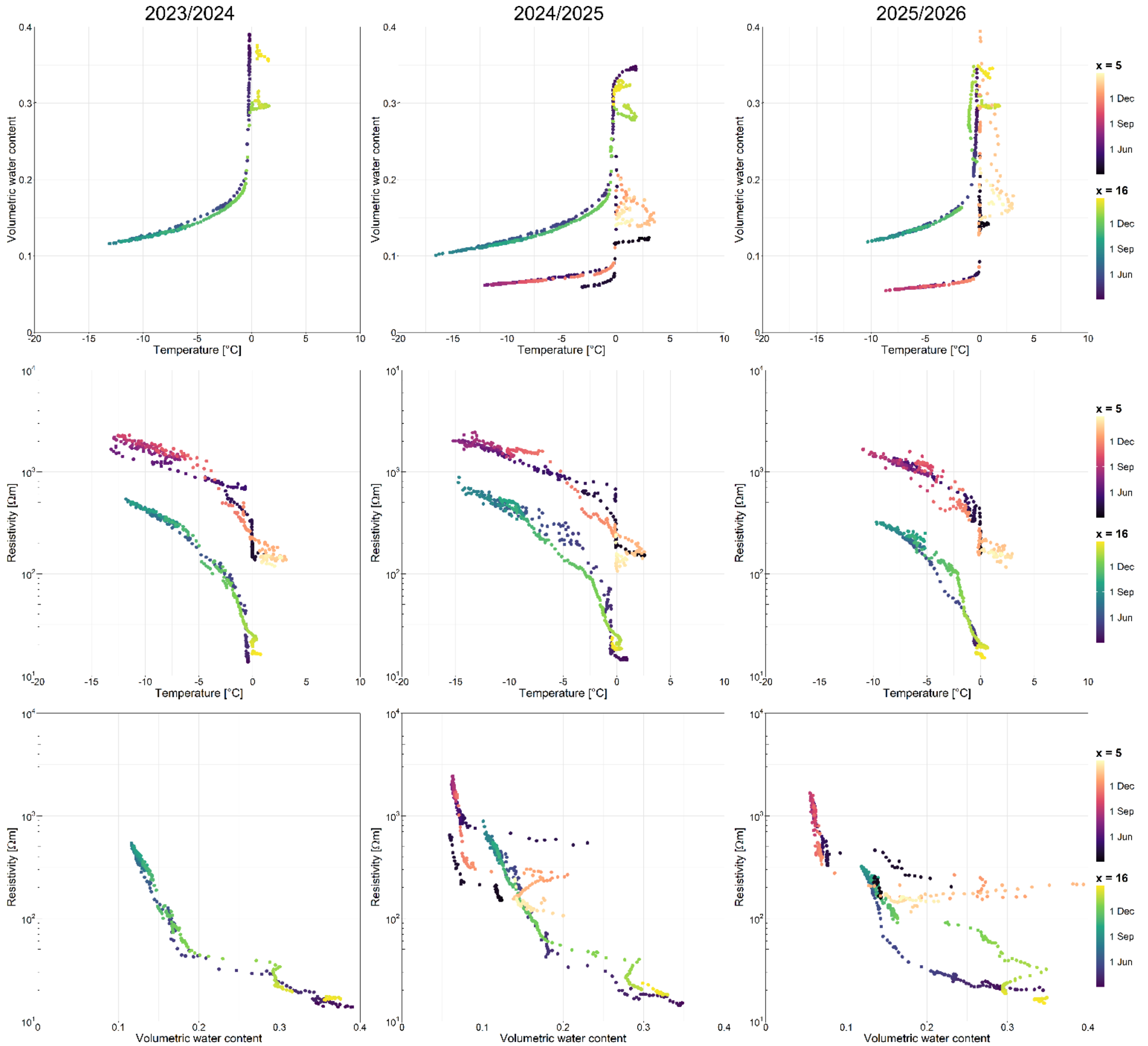

495 **Figure 10: Relationships between resistivity, ground temperature, and volumetric water content at 75 cm depth in the two lithologies – marine terrace (x = 5 m) and Cretaceous sediments (x = 16 m).**

https://doi.org/10.5194/egusphere-2026-5161
Preprint. Discussion started: 14 September 2026

4 Discussion

4.1 Temperature, moisture, and resistivity patterns on James Ross Island

Three years of A-ERT monitoring on JRI provide a unique dataset to compare resistivity dynamics across varying climatic conditions and track the evolution of the active layer. From a local climate perspective, the years 2023/2024 and 2025/2026 were among the warmest recorded on JRI, with mean annual air temperature and mean annual ground temperature at 5 cm depth approximately 2 °C above the long-term 2006–2023 baseline; in contrast, 2024/2025 was below this baseline (Kaplan Pastíriková et al., in review). At the same time, ALT at AWS-CALM decreased progressively from summer 2022/2023 (98 cm) to 2025/2026 (84 cm), with the latter being 4 cm below the 2014–2023 mean (Hrbáček et al., 2025). The suppressed ALT in 2025/2026 was likely driven by summer snow cover presence, a phenomenon previously documented at CALM-S JGM (Hrbáček et al., 2021). The effect of snow cover is also visible in the distribution of temperatures at a depth of 75 cm during the winter. The minimum temperatures in the marine terrace, which is covered by snow for a longer time (Fig. 5a), were 2–5 °C higher than in the Cretaceous sediments (Fig. 10).

The electrical resistivity values recorded on JRI are lower compared to other A-ERT sites in Antarctica (Farzamian et al., 2020, 2023), the Arctic (Tomaškovičová and Ingeman-Nielsen, 2024) or mountainous regions (Hauck and Hilbich, 2024), where the permafrost values typically exceed 10^3 to 10^5 Ωm. With respect to the localization of CALM-S JGM in a coastal zone, an effect of salinity might be one of the causes of the observed low resistivities of both the active layer (ca. 15–150 Ωm) and permafrost (30–100 Ωm) during the thawing season. Such low electrical resistivity values are similar to those observed in other coastal areas of Antarctica (Correia et al., 2017) or the Arctic (e.g. Krautblätter et al., 2024).

Low electrical resistivities (500–2000 Ωm) persisted even during the peak winter season. The only other Antarctic A-ERT sites reporting winter resistivity values are located in the South Shetland Islands, specifically Livingston Island (Farzamian et al., 2024b) and Deception Island (Farzamian et al., 2024a), where winter values commonly exceed 10^5 Ωm. This sharp contrast stems primarily from differing lithologies. While the South Shetland sites consist predominantly of volcanic bedrock and coarse debris, JRI is underlain by fine-grained sedimentary rocks. The finer soil texture on JRI promotes higher moisture retention, sustaining high unfrozen water contents at sub-zero temperatures. Despite the overall low resistivities on JRI, the ratio of unfrozen to frozen resistivity (15–20 for sandy soil and 20–30 for silty soil) remains typical for permafrost environments (Hauck and Hilbich, 2024).

4.2 Role of lithology and snow cover

The A-ERT profile on JRI spans a major lithological boundary, capturing differing electrical signatures across two distinct soil types (Tab. 1) that respond differently to atmospheric and ground thermal fluctuations, moisture, and result in different active layer thickness (Hrbáček et al., 2025). Previous studies conducted on CALM-S JGM utilizing ground-penetrating radar (GPR) and electromagnetic induction (EMI) successfully delineated this boundary; however, those techniques managed to only detect the active layer/permafrost boundary within the Holocene marine sediments, failing to penetrate the deeper

https://doi.org/10.5194/egusphere-2026-5161
Preprint. Discussion started: 14 September 2026

subsurface or detect this boundary within the finer-grained Cretaceous sediments (Hrbáček et al., 2019; 2021). Identifying the active layer/permafrost interface across both lithologies therefore represented a key objective for the A-ERT deployment (cf. Farzamian et al., 2023).

The 2D tomograms clearly resolve the lithological boundary under isothermal conditions (Fig. 8c), which minimize the thermal noise. The higher resistivities (>1500 Ωm) detected in the marine terrace zone reflect a combination of higher ice content and lower measured unfrozen water content in the sandy substrate (Fig. 5). In contrast, resistivities in the Cretaceous sediment zone range between 200 and 500 Ωm and are driven by a finer grain fraction (Tab. 1) and higher unfrozen water content (Fig. 10). This spatial divergence persists during the onset of autumn freezing (Fig. 8a) and peak winter conditions (Fig. 8b), but becomes less pronounced during summer thaw (Fig. 8d–f).

Notably, the northern part of the transect is also under a stronger influence of snow cover, but quantifying the isolated thermal and hydrological impacts of snow cover remains challenging due to the absence of control conditions. Analysis of snow presence confirms its high heterogeneity and uneven distribution, which complicates the process of estimating average snow depth based on camera footage (Fig. 6). Theoretically, a continuous snowpack should lead to a resistivity decrease as it insulates the subsurface and increases meltwater infiltration (e.g. Hilbich et al., 2011; Farzamian et al., 2023). However, this part of the transect has generally higher resistivity values than the southern part consisting of Cretaceous sediments. The occurrence of sharp, high-amplitude resistivity spikes during peak winter suggests that severe ground cooling and freezing proceed despite snow cover, since the usually thin snow depths typically recorded on JRI are insufficient to achieve complete thermal insulation. The increased soil moisture from meltwater infiltration is also strongly constrained by substrate properties. Rather than promoting moisture accumulation, the high permeability of the coarse sandy substrate facilitates rapid vertical drainage and lateral runoff away from the monitoring transect, as evidenced by the downslope saturation zones in Fig. 6d. Consequently, while the influences of lithology and seasonal snow cover on electrical resistivity are closely intertwined, lithological characteristics emerge as the primary driver of the observed resistivity contrasts across the transect. The principal exception occurs during transient melt events, when partially thawed snow refreezes to form an icy surficial layer. These localized refreezing phenomena primarily manifest as abrupt, short-term resistivity shifts very close to the surface rather than broad modulations of the deeper ground thermal regime.

The contrast between the two lithologies complicates the ALT identification in the northern segment of the transect (Fig. 8f, Fig. 9). The sandy material of the marine terrace (ca. 1–1.5 m thick) overlies the Cretaceous sediments along this section, promoting rapid water infiltration through coarser pore networks. During the thawing season, soil water percolates downward (Fig. 5c) until it reaches the permafrost table, occurring usually at a depth of 60–80 cm in this part of the CALM-S JGM grid (Hrbáček et al., 2025). Moisture accumulates at the base of the active layer, freezes at the end of the thawing season, and forms an ice-rich basal layer, whose presence was well detectable by GPR (Hrbáček et al., 2021). Furthermore, the soil texture analysis showed that the surficial layer has 2–4 times higher silt and clay content than the deeper parts of the active layer. This texture change causes some contrast between the 0–20 cm layer (ca. 80–100 Ωm) and 50–80 cm layer (ca. 100–150 Ωm) observed during the peak summer. This contrast is detected by the resistivity gradient method (Fig. 9) which was used for ALT

https://doi.org/10.5194/egusphere-2026-5161
Preprint. Discussion started: 14 September 2026

estimation. The known boundary between the active layer and permafrost is therefore not possible to detect with the A-ERT as it falls within the expected zone of the lithological boundary. The underlying Cretaceous sediments at a depth of 150 cm average ~40 Ωm, even at temperatures below −2 °C (Fig. 8e). Such an inverted resistivity gradient, where permafrost exhibits lower resistivity than the active layer, runs counter to typical resistivity distribution (Hauck and Hilbich, 2024) and precludes an ALT estimate using ERT alone, such as with the resistivity gradient method (Herring and Lewkowicz, 2022).

In contrast, moisture distribution within the Cretaceous sediments is far more uniform, and the vertical resistivity gradient closely mirrors the ground temperature profile, which is well documented in virtual borehole x = 16 m (Fig. 9). The uniform moisture profile and absence of lithological stratification within the Cretaceous domain allow approximate tracking of the thaw front progression and ALT estimation via gradient analysis (Fig. 9).

4.3 Links between ground properties and resistivity

While the A-ERT monitoring yields valuable insights into coupled hydrothermal dynamics within the active layer and permafrost (Tomaškovičová and Ingeman-Nielsen, 2024), disentangling these competing influences remains challenging. Delineating the precise active layer/permafrost interface is complicated not only by the inversion resolution, but primarily by the continuous nature of phase transitions, where ice, water, and temperature change gradually rather than step-wise across heterogeneous lithologies (Fig. 10). Hrbáček et al. (2023b) documented a freezing point depression of up to −0.4 °C at 50 cm depth within the marine terrace. Resistivity-temperature-moisture relationship plots confirm this finding (Fig. 10), yielding estimated freezing points of −0.3 °C for the zone of Cretaceous sediments and −0.1 °C for the marine terrace zones.

The integration of resistivity data provides more detailed constraints on ground freezing and thawing on JRI, determined as the initial and terminal phases of the zero-curtain period. For example, the initial temperature of the zero-curtain in the thawing phase is typically closer to 0 °C than the temperature at the end of freezing zero-curtain (e.g. Teng et al., 2024), which is also documented in Fig. 10. From a physical perspective, the lower temperature limit of the zero-curtain period is more critical than just the freezing point temperature, as it marks the almost full release of latent heat and the onset of sensible cooling/warming. The values of the observed parameters at the end of the zero-curtain period at a depth of 75 cm are −0.7 °C, 0.2 cm³/cm³, 20–35 Ωm, and −0.2 °C, 0.1 cm³/cm³, and 150–250 Ωm within the Cretaceous sediments and the marine terrace sediments, respectively. The scattering of the temperature, moisture, and resistivity values within the marine terrace sediments is a joint artifact of inversion (e.g. Tomaškovičová and Ingeman-Nielsen, 2024) and the principle of TDR measurement.

The general definition of the relationships between ground temperature, moisture, and resistivity is further key for the interpretation of the observed increase of resistivity values especially in the surficial part of the profile between 2023/2024 and 2025/2026 (Fig. 8, 9). The minimum ground temperature at the depth of 5 cm was 4–6 °C higher than in the previous years (Fig. 9) which led to a noticeable decrease of maximum resistivity values during winter.

Across the spatial grid of CALM-S JGM, a distinct active layer pattern emerges (Hrbáček et al., 2025). Thaw depths are consistently deeper in the fine-grained Cretaceous sediments (~90–110 cm) than in the sandy marine terrace (~60–70 cm), most likely due to differences in soil thermal properties (Hrbáček et al., 2017, 2025). At the position of virtual borehole x =

https://doi.org/10.5194/egusphere-2026-5161
Preprint. Discussion started: 14 September 2026

16 m, the freezing threshold was estimated at 35–45 Ωm, corresponding to an ALT of 110–160 cm (Fig. 9a). Notably, this resistivity-derived ALT is 20–60 cm deeper than the position of the 0 °C isotherm, supporting the hypothesis that the physical thawing occurs below the freezing point.

At x = 5 m (Holocene terrace), the freezing resistivity threshold was estimated at a larger range of 150–250 Ωm. However, maximum seasonal thaw depth cannot be reliably determined from the resistivity gradient in this profile segment. Although a sharp resistivity gradient between frozen and unfrozen ground appears briefly at the start of thaw, it degrades rapidly as summer progresses. Thinning of the basal ice layer combined with the lower baseline resistivity of the underlying Cretaceous sediment causes the signal boundary to blur within the inversion model (Fig. 9).

4.4 Overall performance of A-ERT on James Ross Island

The first A-ERT sites using Lippmann instrumentation were established in rather homogeneous grounds in the South Shetland Islands (Farzamian et al., 2020, 2024a, 2024b). Thus, the A-ERT system at CALM-S JGM was purposefully deployed across a lithologically more complex transect to test the limits of the method for detecting active layer freezing and thawing processes. The quality-control and filtering procedure resulted in the exclusion of only a small number of measurements from each dataset, and no dataset was excluded from the process. Typically, just 1–7 measurements were removed from each dataset, corresponding to less than approximately 2% of the measurements. This low rejection rate indicates consistently high data quality and suggests that good electrode–ground contact was maintained throughout the monitoring period, despite the challenging conditions associated with frozen ground. The inversion results also showed a consistent level of fit over time, with RMS errors generally remaining within the range of 4–8%. Such relatively low and stable RMS values indicate a good correspondence between the measured apparent resistivities and those predicted by the inversion models.

As discussed in Section 4.1, the selected site is characterized by very low permafrost resistivities. In combination with the lithological heterogeneity, this complicates data interpretation because the lithological contrast suppresses the electrical resistivity signal between frozen and unfrozen material. Potential interpretation uncertainties were partially mitigated by robust ground-truth data, including ground temperature, moisture, and texture analysis for both lithological units. Combined with resistivity data, these measurements enabled a more precise estimation of the freezing point as well as the initial and terminal temperatures of the zero-curtain period.

As stated above, one of the primary objectives of A-ERT was to track the seasonal evolution of thaw depth, particularly within the Cretaceous sediments where GPR and EMI had previously failed to provide reliable results (Hrbáček et al., 2019, 2021). For this purpose, the resistivity gradient method (Herring and Lewkowicz, 2022) was applied. This approach performed well in the Cretaceous portion of the profile, providing ALT estimates where GPR and EMI failed, even though it overestimates the thaw depth due to the possible effects of pore size and salinity. Conversely, the gradient method is not suitable for the marine terrace section, where it incorrectly identifies the textural boundary between the fine-grained surface layer and the underlying sandier material as the thaw front. Consequently, obtaining direct temperature or moisture data from depths below 75 cm in the left part of the profile would be highly beneficial to clarify the thermal regime at the underlying Cretaceous

https://doi.org/10.5194/egusphere-2026-5161
Preprint. Discussion started: 14 September 2026

boundary. Furthermore, decreasing the electrode spacing in future deployments could increase spatial detail and help to resolve these shallow, multi-layered textural contrasts.

Although the A-ERT system did not fully resolve every operational challenge, it provided novel and critical insights, advancing our understanding of active layer freezing and thawing dynamics at CALM-S JGM. This research demonstrates that in highly heterogeneous substrates, ground-truth data (at least for ground temperature and moisture) are indispensable for site-specific geophysical interpretation.

5 Summary and conclusions

Three years of continuous A-ERT monitoring on James Ross Island provided novel insights into the application of A-ERT for active layer and permafrost research and site-specific information improving the knowledge of the long-term active layer monitoring site CALM-S JGM.

The results confirmed the original hypothesis that the contrasts along the monitoring profile are primarily governed by lithological differences and moisture dynamics. The sandy Holocene marine terrace promotes rapid drainage and faster initial thaw propagation, resulting in sharp seasonal resistivity transitions. Conversely, fine-grained, clay-rich sediments of the Cretaceous Whisky Bay Formation retain moisture efficiently, leading to a more gradual, but deeper thaw penetration governed by higher water retention capacity and thermal inertia. Site-specific conditions induce an inverted resistivity gradient in the sandy marine terrace section (higher active layer resistivities overlying lower permafrost resistivities), which prevents gradient-based estimation of ALT in that portion of the profile.

Finally, joint analysis of resistivity, ground temperature, and volumetric water content datasets clarified key phase-change characteristics across these contrasting lithologies:

1. Freezing point depression was detected at −0.3 °C in the Cretaceous sediments and at −0.1 °C in the marine terrace deposits.
2. Physical freezing onset (zero-curtain end) with almost complete water-to-ice phase change and sensible cooling initiated at −0.7 °C (25–35 Ωm) in Cretaceous sediments, compared to −0.3 °C (150–250 Ωm) in the marine terrace.

Author contributions

MK – formal analysis, visualization, writing (original draft); MF – conceptualization, formal analysis, writing (review and editing); FH – funding acquisition, methodology, resources, writing (original draft); TH – data curation, resources, writing (review and editing); TU – investigation, writing (review and editing); CH – conceptualization, funding acquisition, writing (review and editing)

https://doi.org/10.5194/egusphere-2026-5161
Preprint. Discussion started: 14 September 2026

Competing interests

At least one of the (co-)authors is a member of the editorial board of The Cryosphere.

Acknowledgements

The authors acknowledge the Czech Antarctic Research Programme for logistical support. During the preparation of this manuscript, Gemini 3.1 Pro was utilized to improve the structure and readability of the text, as well as to ensure consistent spelling, grammar, and punctuation. The authors have reviewed the edits and take full responsibility for the content of the publication.

Financial support

The research was funded by Ministry of Education, Youth and Sports of Czech Republic project (LL2505) and Czech Science Foundation projects GM22-28659M and GA25-18272S. The installation of A-ERT system was funded by the Swiss Polar Institute grant (SPI Technogrant: TEG-2021-003: ERT-PERM). FH acknowledges PermaCOST (COST Action project CA24157) for the funding of a short-term scientific mission at the University of Fribourg.

References

Biskaborn, B. K., Smith, S. L., Noetzli, J., Matthes, H., Vieira, G., Streletskiy, D. A., Schoeneich, P., Romanovsky, V. E., Lewkowicz, A. G., Abramov, A., Allard, M., Boike, J., Cable, W. L., Christiansen, H. H., Delaloye, R., Diekmann, B., Drozdov, D., Etzelmüller, B., Grosse, G., Guglielmin, M., Ingeman-Nielsen, T., Isaksen, K., Ishikawa, M., Johansson, M., Johannsson, H., Joo, A., Kaverin, D., Kholodov, A., Konstantinov, P., Kröger, T., Lambiel, C., Lanckman, J. P., Luo, D., Malkova, G., Meiklejohn, I., Moskalenko, N., Oliva, M., Phillips, M., Ramos, M., Sannel, A. B. K., Sergeev, D., Seybold, C., Skryabin, P., Vasiliev, A., Wu, Q., Yoshikawa, K., Zheleznyak, M., and Lantuit, H.: Permafrost is warming at a global scale, Nat. Commun., 10, 1042, https://doi.org/10.1038/s41467-018-08240-4, 2019.

Bockheim, J., Vieira, G., Ramos, M., López-Martínez, J., Serrano, E., Guglielmin, M., Wilhelm, K., and Nieuwendam, A.: Climate warming and permafrost dynamics in the Antarctic Peninsula region, Glob. Planet. Change, 100, 215–223, https://doi.org/10.1016/j.gloplacha.2012.10.018, 2013.

Brooks, S. T., Jabour, J., van den Hoff, J., and Bergstrom, D. M.: Our footprint on Antarctica competes with nature for rare ice-free land, Nat. Sustain., 2, 185–190, https://doi.org/10.1038/s41893-019-0237-y, 2019.

Brown, J., Nelson, F. E., and Hinkel, K. M.: The circumpolar active layer monitoring (CALM) program research designs and initial results, Polar Geogr., 24 (3), 165–258, https://doi.org/10.1080/10889370009377698, 2000.

https://doi.org/10.5194/egusphere-2026-5161
Preprint. Discussion started: 14 September 2026

Burn, C. R.: The active layer: Two contrasting definitions, Permafrost Periglac. Process., 9, 411–416, https://doi.org/10.1002/(SICI)1099-1530(199810/12)9:4<411::AID-PPP292>3.0.CO;2-6, 1998.

Correia, A., Oliva, M., and Ruiz-Fernández, J.: Evaluation of frozen ground conditions along a coastal topographic gradient at Byers Peninsula (Livingston Island, Antarctica) by geophysical and geoecological methods, Catena, 149, 529–537, https://doi.org/10.1016/j.catena.2016.08.006, 2017.

Devoie, É. G., Gruber, S., and McKenzie, J. M.: A repository of measured soil freezing characteristic curves: 1921 to 2021, Earth Syst. Sci. Data, 14, 3365–3377, https://doi.org/10.5194/essd-14-3365-2022, 2022.

Farzamian, M., Vieira, G., Monteiro Santos, F. A., Yaghoobi Tabar, B., Hauck, C., Catarina Paz, M., Bernardo, I., Ramos, M., and Angel De Pablo, M.: Detailed detection of active layer freeze–thaw dynamics using quasi-continuous electrical resistivity tomography (Deception Island, Antarctica), The Cryosphere, 14, 1105–1120, https://doi.org/10.5194/tc-14-1105-2020, 2020.

Farzamian, M., Blanchy, G., McLachlan, P., Vieira, G., Esteves, M., de Pablo, M. A., Triantifilis, J., Lippmann, E., and Hauck, C.: Advancing permafrost monitoring with autonomous electrical resistivity tomography (A-ERT): Low-cost instrumentation and open-source data processing tool (v1.0.0), Zenodo [software], https://doi.org/10.5281/zenodo.10183126, 2023.

Farzamian, M., Blanchy, G., McLachlan, P., Vieira, G., Esteves, M., de Pablo, M. A., Triantifilis, J., Lippmann, E., and Hauck, C.: Advancing permafrost monitoring with autonomous electrical resistivity tomography (A-ERT): Low-cost instrumentation and open-source data processing tool, Geophys. Res. Lett., 51, e2023GL105770, https://doi.org/10.1029/2023GL105770, 2024a.

Farzamian, M., Herring, T., Vieira, G., de Pablo, M. A., Yaghoobi Tabar, B., and Hauck, C.: Employing automated electrical resistivity tomography for detecting short- and long-term changes in permafrost and active-layer dynamics in the maritime Antarctic, The Cryosphere, 18, 4197–4213, https://doi.org/10.5194/tc-18-4197-2024, 2024b.

Guglielmin, M.: Ground surface temperature (GST), active layer, and permafrost monitoring in continental Antarctica, Permafrost Periglac. Process., 17, 133–143, https://doi.org/10.1002/ppp.553, 2006.

Guglielmin, M. and Cannone, N.: A permafrost warming in a cooling Antarctica? Clim. Change, 111, 177–195, https://doi.org/10.1007/s10584-011-0137-2, 2012.

Günther, T., Rücker, C., and Spitzer, K.: Three-dimensional modelling and inversion of DC resistivity data incorporating topography—II. Inversion, Geophys. J. Int., 166, 506–517, https://doi.org/10.1111/j.1365-246X.2006.03011.x, 2006.

Hauck, C.: Frozen ground monitoring using DC resistivity tomography, Geophys. Res. Lett., 29, 2016, https://doi.org/10.1029/2002GL014995, 2002.

Hauck, C. and Hilbich, C.: Preconditioning of mountain permafrost towards degradation detected by electrical resistivity, Environ. Res. Lett., 19, 064010, https://doi.org/10.1088/1748-9326/ad3c55, 2024.

Herring, T. and Lewkowicz, A. G.: A systematic evaluation of electrical resistivity tomography for permafrost interface detection using forward modeling, Permafrost Periglac. Process., 33, 134–146, https://doi.org/10.1002/ppp.2141, 2022.

https://doi.org/10.5194/egusphere-2026-5161
Preprint. Discussion started: 14 September 2026

Herring, T., Lewkowicz, A. G., Hauck, C., Hilbich, C., Mollaret, C., Oldenborger, G. A., Uhlemann, S., Farzamian, M., Calmels, F., and Scandroglio, R.: Best practices for using electrical resistivity tomography to investigate permafrost, Permafrost Periglac. Process., 34, 36–51, https://doi.org/10.1002/ppp.2207, 2023

Hilbich, C., Hauck, C., Hoelzle, M., Scherler, M., Schudel, L., Völksch, I., Vonder Mühll, D., and Mäusbacher, R.: Monitoring mountain permafrost evolution using electrical resistivity tomography: A 7-year study of seasonal, annual, and long-term variations at Schilthorn, Swiss Alps, J. Geophys. Res., 113, F01S90, https://doi.org/10.1029/2007JF000799, 2008.

Hilbich, C., Fuss, C., and Hauck, C.: Automated time-lapse ERT for improved process analysis and monitoring of frozen ground, Permafrost Periglac. Process., 22, 306–319, https://doi.org/10.1002/ppp.732, 2011.

Hrbáček, F., Kňažková, M., Nývlt, D., Láska, K., Mueller, C. W., and Ondruch, J.: Active layer monitoring at CALM-S site near J.G. Mendel station, James Ross Island, eastern Antarctic Peninsula, Sci. Total Environ., 601–602, 987–997, https://doi.org/10.1016/j.scitotenv.2017.05.266, 2017.

Hrbáček, F., Nývlt, D., Láska, K., Kňažková, M., Kampová, B., Engel, Z., Oliva, M., and Mueller, C. W.: Permafrost and active layer research on James Ross Island: An overview, Czech Polar Rep., 9, 20–36, https://doi.org/10.5817/CPR2019-1-3, 2019.

Hrbáček, F., Engel, Z., Kňažková, M., and Smolíková, J.: Effect of summer snow cover on the active layer thermal regime and thickness on CALM-S JGM site, James Ross Island, eastern Antarctic Peninsula, Catena, 207, 105608, https://doi.org/10.1016/j.catena.2021.105608, 2021.

Hrbáček, F., Oliva, M., Hansen, C., Balks, M., O'Neill, T. A., de Pablo, M. A., Ponti, S., Ramos, M., Vieira, G., Abramov, A., Kaplan Pastíriková, L., Guglielmin, M., Goyanes, G., Francelino, M. R., Schaefer, C., and Lacelle, D.: Active layer and permafrost thermal regimes in the ice-free areas of Antarctica, Earth-Sci. Rev., 242, 104458, https://doi.org/10.1016/j.earscirev.2023.104458, 2023a.

Hrbáček, F., Kňažková, M., Farzamian, M., and Baptista, J.: Variability of soil moisture on three sites in the Northern Antarctic Peninsula in 2022/23, Czech Polar Rep., 13, 10–23, https://doi.org/10.5817/CPR2023-1-2, 2023b.

Hrbáček, F., Kňažková, M., Láska, K., and Pastíriková, L.: Active layer warming and thickening on CALM-S JGM, James Ross Island, in the period 2013/14–2022/23, Permafrost Periglac. Process., 36, 378–389, https://doi.org/10.1002/ppp.2274, 2025.

Kaplan Pastíriková, L., Hrbáček, F., Uxa, T., and Láska, K.: Permafrost table temperature and active layer thickness variability on James Ross Island, Antarctic Peninsula, in 2004–2021, Sci. Total Environ., 869, 161690, https://doi.org/10.1016/j.scitotenv.2023.161690, 2023.

Kaplan Pastíriková, L., Hrbáček, F., Matějka, M., Kňažková, M., and Uxa, T.: Reconstruction of permafrost table temperature and active layer thickness on James Ross Island, Antarctic Peninsula (1979–2023), Permafrost Periglac. Process., submitted.

Kavan, J., Nývlt, D., Láska, K., Engel, Z., and Kňažková, M.: High-latitude dust deposition in snow on the glaciers of James Ross Island, Antarctica, Earth Surf. Process. Landf., 45, 1569–1578, https://doi.org/10.1002/esp.4831, 2020.

https://doi.org/10.5194/egusphere-2026-5161
Preprint. Discussion started: 14 September 2026

Krautblätter, M., Angelopoulos, M., Pollard, W. H., Lantuit, H., Lenz, J., Fritz, M., Couture, N., and Eppinger, S.: Life cycles and polycyclicity of mega retrogressive thaw slumps in Arctic permafrost revealed by 2D/3D geophysics and long-term retreat monitoring, J. Geophys. Res. Earth Surf., 129, e2023JF007556, https://doi.org/10.1029/2023JF007556, 2024.

Lee, J. R., Raymond, B., Bracegirdle, T. J., Chadès, I., Fuller, R. A., and Shaw, J. D.: Climate change drives expansion of Antarctic ice-free habitat, Nature, 547, 49–54, https://doi.org/10.1038/nature22996, 2017.

Loke, M. H.: Tutorial: 2D and 3D electrical imaging surveys, 2nd edn., Geotomo Software, [2002.

Mlčoch, B., Nývlt, D., and Mixa, P. (Eds.): Geological map of James Ross Island—Northern part 1:25,000, Czech Geological Survey, 2020.

Obu, J.: How much of the Earth's surface is underlain by permafrost?, J. Geophys. Res. Earth Surf., 126, e2021JF006123, https://doi.org/10.1029/2021JF006123, 2021.

Roman, M., Nývlt, D., Davies, B. J., Braucher, R., Jennings, S. J. A., Břežný, M., Glasser, N. F., Hambrey, M. J., Lirio, J. M., and Rodés, Á.: Accelerated retreat of northern James Ross Island ice streams (Antarctic Peninsula) in the Early-Middle Holocene induced by buoyancy response to postglacial sea level rise, Earth Planet. Sci. Lett., 641, 118803, https://doi.org/10.1016/j.epsl.2024.118803, 2024.

Romanovsky, V. E., Smith, S. L., and Christiansen, H. H.: Permafrost thermal state in the polar Northern Hemisphere during the International Polar Year 2007–2009: A synthesis, Permafrost Periglac. Process., 21, 106–116, https://doi.org/10.1002/ppp.689, 2010.

Rücker, C., Günther, T., and Wagner, F. M.: pyGIMLi: An open-source library for modelling and inversion in geophysics, Comput. Geosci., 109, 106–123, https://doi.org/10.1016/j.cageo.2017.07.011, 2017.

Stringer, C. D., Carrivick, J. L., Quincey, D. J., Nývlt, D., and Comber, A.: Land cover change across the major proglacial regions of the sub-Antarctic islands, Antarctic Peninsula, and McMurdo Dry Valleys, during the 21st century, Arct. Antarct. Alp. Res., 57(1), 2483474, https://doi.org/10.1080/15230430.2025.2483474, 2025.

Teng, J., Dong, A., Zhang, S., Zhang, X., and Sheng, D.: Freezing-thawing hysteretic behavior of soils, Water Resour. Res., 60, e2024WR037280, https://doi.org/10.1029/2024WR037280, 2024.

Tomaškovičová, S. and Ingeman-Nielsen, T.: Quantification of freeze–thaw hysteresis of unfrozen water content and electrical resistivity from time lapse measurements in the active layer and permafrost, Permafrost Periglac. Process., 35, 79–97, https://doi.org/10.1002/ppp.2201, 2024.

Tso, C.-H. M., Kuras, O., Wilkinson, P. B., Uhlemann, S., Chambers, J. E., Meldrum, P. I., Graham, J., Sherlock, E. F., and Binley, A.: Improved characterisation and modelling of measurement errors in electrical resistivity tomography (ERT) surveys, J. Appl. Geophys., 146, 103–119, https://doi.org/10.1016/j.jappgeo.2017.09.009, 2017.

Turner, J., Marshall, G., Clem, K., Colwell, S., Phillips, T., and Lu, H.: Antarctic temperature variability and change from station data, Int. J. Climatol., 40, 2986–3007, https://doi.org/10.1002/joc.6378, 2020.

https://doi.org/10.5194/egusphere-2026-5161
Preprint. Discussion started: 14 September 2026

van Wessem, J. M., Ligtenberg, S. R. M., Reijmer, C. H., van den Berg, W. J., van den Broeke, M. R., Barrand, N. E., Thomas, E. R., Turner, J., Wuite, J., Scambos, T. A., and van Meijgaard, E.: The modelled surface mass balance of the Antarctic Peninsula at 5.5 km horizontal resolution, The Cryosphere, 10, 271–285, https://doi.org/10.5194/tc-10-271-2016, 2016.

Vieira, G., Bockheim, J., Guglielmin, M., Balks, M., Abramov, A. A., Boelhouwers, J., Cannone, N., Ganzert, L., Gilichinsky, D. A., Goryachkin, S., López-Martínez, J., Meiklejohn, I., Raffi, R., Ramos, M., Schaefer, C., Serrano, E., Simas, F., Sletten, R., and Wagner, D.: Thermal state of permafrost and active-layer monitoring in the Antarctic: Advances during the International Polar Year 2007–2009, Permafrost Periglac. Process., 21, 182–197, https://doi.org/10.1002/ppp.685, 2010.

Wang, S., Li, R., Wu, T., Ma, J., Liu, W., Yang, S., Du, Y., Xiao, Y., Wu, X., Hu, G., Yao, J., Tang, S., Zhu, X., Shi, J., and Qiao, Y.: Evaluating the impact of different freezing-point depression equations on permafrost hydrothermal processes in the Arctic and Qinghai-Tibet Plateau with CLM5.0, Agric. For. Meteorol., 379, 111034, https://doi.org/10.1016/j.agrformet.2026.111034, 2026.